



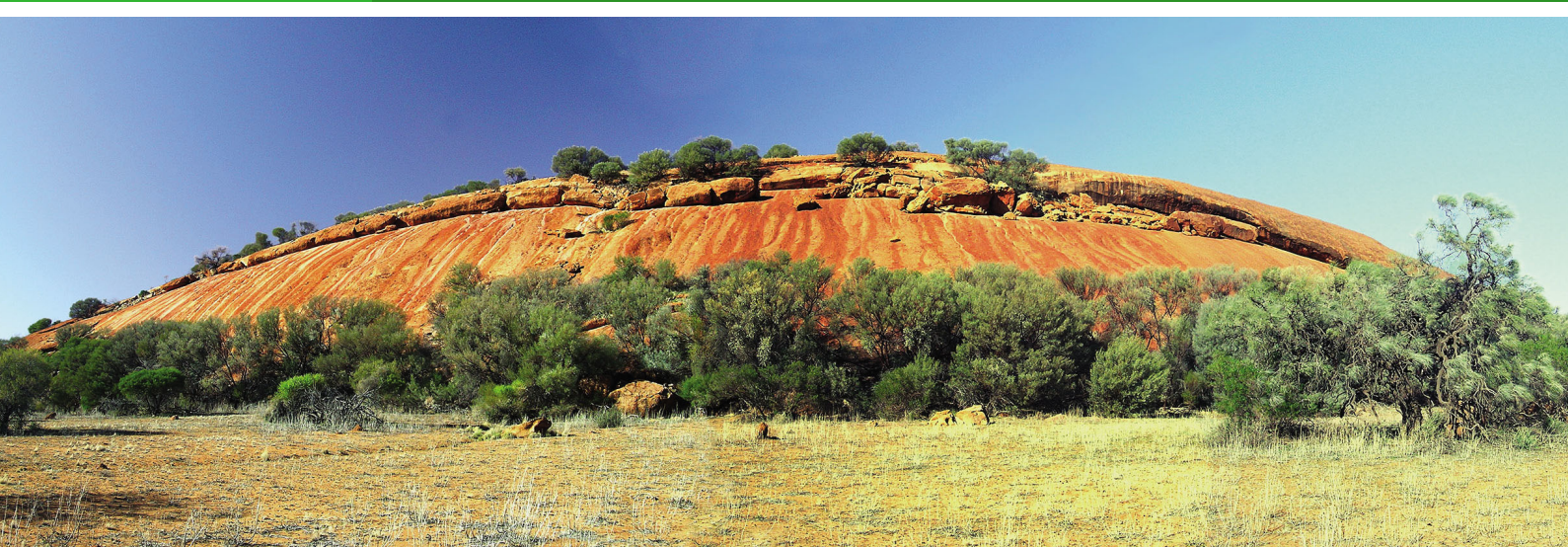
Government of
Western Australia

REPORT 120

Department of
Mines and Petroleum

JUVENILE CRUST FORMATION AND RECYCLING IN THE NORTHERN MURCHISON DOMAIN, YILGARN CRATON: EVIDENCE FROM Hf ISOTOPES AND GRANITE GEOCHEMISTRY

by TJ Ivanic, MJ Van Kranendonk, CL Kirkland,
S Wyche, MTD Wingate and E Belousova



Geological Survey of Western Australia



Government of **Western Australia**
Department of **Mines and Petroleum**

REPORT 120

JUVENILE CRUST FORMATION AND RECYCLING IN THE NORTHERN MURCHISON DOMAIN, YILGARN CRATON: EVIDENCE FROM Hf ISOTOPES AND GRANITE GEOCHEMISTRY

by

**TJ Ivanic, MJ Van Kranendonk², CL Kirkland, S Wyche, MTD Wingate and
EA Belousova¹**

¹ ARC National Key Centre for Geochemical Evolution and Metallogeny of Continents (GEMOC), Department of Earth and Planetary Sciences, Macquarie University, Sydney, NSW 2109, Australia

² School of Biology, Earth and Environment, University of New South Wales, Sydney, NSW 2052, Australia

Perth 2013



**Geological Survey of
Western Australia**

MINISTER FOR MINES AND PETROLEUM

DIRECTOR GENERAL, DEPARTMENT OF MINES AND PETROLEUM

Richard Sellers

EXECUTIVE DIRECTOR, GEOLOGICAL SURVEY OF WESTERN AUSTRALIA

Rick Rogerson

REFERENCE

The recommended reference for this publication is:

Ivanic, T.J., Van Kranendonk, M.J., Kirkland, C.L., Wyche, S., Wingate, M.T.D. and Belousova, E.A. 2013, Juvenile crust formation and recycling in the northern Murchison domain, Yilgarn Craton: evidence from Hf isotopes and granite geochemistry: Geological Survey of Western Australia, Report 120, 34p.

National Library of Australia Cataloguing-in-Publication entry

Author: Ivanic, T.J.

Title: Juvenile crust formation and recycling in the northern Murchison domain, Yilgarn Craton [electronic resource] : evidence from HF isotopes and granite geochemistry / T.J. Ivanic, M.J. Van Kranendonk, C.L. Kirkland, S. Wyche, M.T.D. Wingate, E.A. Belousova.

ISBN: 9781741684841 (ebook)

Subjects: Geology, Structural--Western Australia--Yilgarn Craton. Soil crusting--Western Australia--Yilgarn Craton. Cratons--Western Australia--Yilgarn Craton. Earth--Crust.

Other Authors/Contributors: Van Kranendonk, Martin Julian, 1962-
Kirkland, C. L.
Wyche, S.
Wingate, M. T. D. (Michael Thomas David)
Belousova, E. A.

Dewey Number: 551.7

ISSN 0508-4741

Grid references in this publication refer to the Geocentric Datum of Australia 1994 (GDA94). Locations mentioned in the text are referenced using Map Grid Australia (MGA) coordinates, Zone 50. All locations are quoted to at least the nearest 100 m.



U–Pb measurements were conducted using the SHRIMP II ion microprobes at the John de Laeter Centre of Isotope Research at Curtin University in Perth, Australia. Isotope analyses were funded in part by the Western Australian government Exploration Incentive Scheme (EIS). Lu–Hf measurements were conducted using LA-ICPMS at the ARC National Key Centre for Geochemical Evolution and Metallogeny of Continents (GEMOC), via the ARC Centre of Excellence in Core to Crust Fluid Systems (CCFS), based in the Department of Earth and Planetary Sciences at Macquarie University, Australia.

Copy editor: K Hawkins
Cartography: CS Schroder
Desktop publishing: RL Hitchings
Printed by Images on Paper, Perth, Western Australia

Published 2013 by Geological Survey of Western Australia

This Report is published in digital format (PDF), as part of a digital dataset, and is available online at <http://www.dmp.wa.gov.au/GSWApublications>.

Further details of geological publications and maps produced by the Geological Survey of Western Australia are available from:

Information Centre
Department of Mines and Petroleum
100 Plain Street
EAST PERTH WESTERN AUSTRALIA 6004
Telephone: +61 8 9222 3459 Facsimile: +61 8 9222 3444
www.dmp.wa.gov.au/GSWApublications

Cover photograph: Exfoliating dome of K-feldspar megacrystic monzogranite of the Bald Rock Supersuite at Walga Rock on Noondie (MGA Zone 50 J 546994E 6969624N)

Contents

Abstract	1
Introduction	1
Geological setting	2
Greenstones	2
Granitic rocks	5
Nomenclature and comparison to previously identified granitic suites	5
Analytical methods	6
Geochemical data	6
Isotopic data	6
Results	7
Lu–Hf and U–Pb data	7
Summary of samples with Lu–Hf and U–Pb data	7
Whole-rock geochemical data	9
Annean Supersuite	9
Big Bell Suite	10
Jungar and Tuckanarra Suites	10
Bald Rock Supersuite	10
Lu–Hf isotope data	11
Discussion	13
Previous work	13
Interpretation of geochemical data	13
Interpretation of Lu–Hf isotope data	17
Implications for Archean granite genesis	20
Relation to seismic data	20
Conclusions	20
Acknowledgements	21
References	21

Appendix

Analytical results and geochemical model	25
Table A1.1. Major and trace element geochemistry for northern Murchison Domain samples	27
Table A1.2. Lu–Hf analytical data for northern Murchison Domain zircon samples	29
Table A1.3. Major and trace element modelling for generation of the Cullculli Suite	33

Figures

1. Simplified geological map of the Yilgarn Craton showing major terrane subdivisions	2
2. Simplified geological map of the northeastern Murchison Domain, highlighting the locations for Lu–Hf samples and the distribution of granitic suites and supersuites	3
3. Stratigraphic scheme for the Murchison Domain, divided into two main columns for supracrustal and magmatic rocks	4
4. Hf isotope plots for zircons from the northern Murchison Domain samples in this study	12
5. Primitive mantle (PM)-normalized rare earth element plots	14
6. Primitive mantle-normalized trace element diagrams	15
7. Trace element plots for the granitic suites of the northern Murchison Domain	16
8. Trace element compositions for the result of mixing Meekatharra Formation basalt and Annean Supersuite granodiorite	17
9. Summary tectonic evolution diagram	19

Tables

1. Classifications of granitic suites from this study compared with those in previous studies	6
---	---

Juvenile crust formation and recycling in the northern Murchison Domain, Yilgarn Craton: evidence from Hf isotopes and granite geochemistry

by

TJ Ivanic, MJ Van Kranendonk², CL Kirkland, S Wyche, MTD Wingate and EA Belousova¹

Abstract

New in situ Lu–Hf data on zircons from GSWA geochronology samples have provided a unique isotopic dataset with high temporal resolution for the Murchison Domain of the Yilgarn Craton in Western Australia. These data identify extended periods of juvenile mantle input (positive ϵHf values) into the crust first at c. 2980 Ma and then from c. 2820 Ma to c. 2640 Ma with significant pulses of crustal recycling at c. 2750 Ma and c. 2620 Ma (highly negative ϵHf values). Geochemical data from well-characterized granitic suites of the Murchison Domain provide additional constraints on the crustal evolution of the area and indicate a prolonged period of crustal melting and remelting at progressively shallower depths from c. 2750 to c. 2600 Ma.

At c. 2760–2753 Ma, widespread calc-alkaline, intermediate to silicic volcanic rocks of the Polelle Group were erupted, accompanied by intrusion of felsic to intermediate melts derived from a variety of crustal sources that likely formed by partial mixing with basaltic melts. The intrusive rocks include a wide geochemical array of rocks in the Cullculli and Eelya Suites that were sourced over a wide range of crustal depths. At this time a major departure to negative ϵHf values (< -5) occurred, indicating sampling of c. 3.80 Ga model aged source rocks and continued juvenile input. Post-volcanic granitic rocks emplaced between c. 2710 and c. 2600 Ma show geochemical evidence for progressive fractionation through time and derivation from an evolving crustal source.

We interpret the driving force for this protracted history of mantle and crustal melting to be two mantle plumes at 2.81 and 2.72 Ga. These data document the process of cratonization through progressive melt depletion of the lower crust, progressively fractionated and shallower melts, culminating with a final phase of crustal recycling ($\epsilon\text{Hf} < -5$) and the cessation of juvenile input at c. 2630–2600 Ma during intrusion of the Bald Rock Supersuite, resulting in cratonization of this part of the Yilgarn Craton.

KEYWORDS: crustal evolution, isotope geochemistry, mantle plumes, Lutetium hafnium dating, Lutetium isotopes

Introduction

The approximately 1 000 000-km² Archean Yilgarn Craton, Western Australia, comprises three terranes (Fig 1; Cassidy et al., 2006) — the Narryer, Youanmi, and South West Terranes — and the Eastern Goldfields Superterrane (EGST), an interpreted collage of terranes formed during 2690–2640 Ma subduction, arc magmatism, terrane accretion, and collisional orogeny (Barley et al., 2008; Kositcin et al., 2008; Czarnota et al., 2010). The Ida Fault separates the Youanmi Terrane from the EGST to the east. The Youanmi Terrane is approximately one-third of the area of the Yilgarn Craton and is divided into the Murchison Domain in the west and the Southern Cross

Domain in the east. The Narryer Terrane in the northwest contains the oldest rocks in the Yilgarn Craton and lies in tectonic contact with the Youanmi Terrane (Myers, 1988; Nutman et al., 1993). The South West Terrane has been interpreted as a series of subterrane that accreted to the Yilgarn Craton during the late Neoproterozoic (Wilde et al., 1996).

Recent mapping and newly acquired geochemical and geochronological data have allowed formulation of a new stratigraphic and structural framework for the Murchison Domain, indicative of an autochthonous crustal development from 2820–2600 Ma (Champion and Cassidy, 2002; Van Kranendonk and Ivanic, 2009; Champion and Cassidy, 2010; Van Kranendonk et al., in press). New results from large, widespread mafic–ultramafic layered igneous complexes (Ivanic et al., 2010) and mafic–ultramafic parts of the volcanic stratigraphy (Barley et al., 2000) indicate significant mantle input into Murchison Domain crust from c. 2820 to 2720 Ma. These complexes were emplaced into, and on top of, older crust

¹ ARC National Key Centre for Geochemical Evolution and Metallogeny of Continents (GEMOC), Department of Earth and Planetary Sciences, Macquarie University, Sydney, NSW 2109, Australia

² School of Biology, Earth and Environment, University of New South Wales, Sydney, NSW 2052, Australia

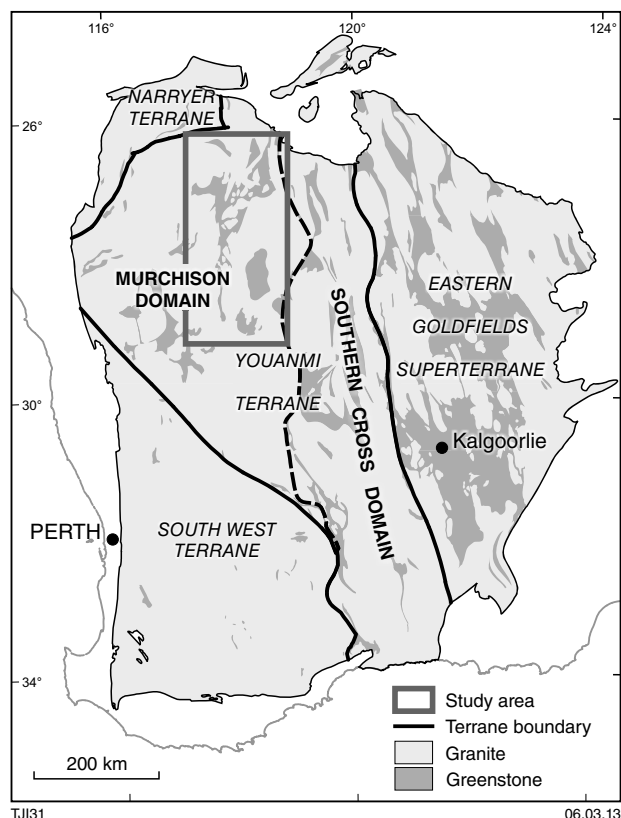


Figure 1. Simplified geological map of the Yilgarn Craton showing major terrane subdivisions (Cassidy et al., 2006), granitic and greenstone distribution, and the location of the study area within the northern Murchison Domain

with a history back to at least c. 2980 Ma and focused along the boundary between the Murchison and Southern Cross Domains (Champion and Cassidy, 2010; Ivanic et al., 2010). The data presented here have also been used to subdivide the widespread granitic rocks of the Murchison Domain into eight well-characterized suites (Figs. 2, 3). These suites incorporate synvolcanic, syntectonic, and post-tectonic granitoids ranging in age between 2815 and 2600 Ma.

Despite these recent advances, several questions remain as to the tectonic setting of crust formation, and the driving forces behind magmatic and structural events. In particular, it is unclear what sources and driving forces are responsible for the long-lived and widespread felsic magmatism in Murchison Domain evolution, and their link to the emplacement of mantle-derived mafic–ultramafic rocks. In order to assess some of these issues, new in situ Lu–Hf data were obtained from zircons from Murchison Domain samples previously dated by the U–Pb sensitive high-resolution ion microprobe (SHRIMP) method. In this Report we show how these data identify extended periods of juvenile mantle input into the crust and how this input was mixed with older crustal source material. The data also enable us to identify the onset of significant crustal recycling at c. 2750 Ma. We supplement this with

geochemical data from well-characterized granitic suites of the Murchison Domain. Collectively, the geochemical and Lu–Hf isotopic data provide additional constraints on the crustal evolution of the Murchison Domain, specifically indicating a prolonged period of crustal melting and remelting at progressively shallower depths from c. 2750 to c. 2600 Ma, supporting a plume-driven and largely in situ crustal development of Murchison Domain over this interval.

Geological setting

Van Kranendonk and Ivanic (2009) formulated a new stratigraphic framework for 2820–2700 Ma supracrustal and layered mafic–ultramafic intrusive rocks, and c. 2800–2600 Ma granitic rocks in the northern Murchison Domain, between Meekatharra and Cue (Figs 2, 3), and for an older succession from c. 2960–2930 Ma in the Golden Grove and Mount Gibson areas (Yeats et al., 1996; Wang et al., 1998). The observation of two regional unconformities between the Golden Grove Group and the Norie Group (Wang et al., 1998) and between the Polelle Group and the Glen Group (Van Kranendonk et al., 2010, locality 2.15), indicate an autochthonous development for the Murchison Domain, which is supported by a lack of significant thrusts exposed anywhere in the northern Murchison Domain.

Greenstones

Four autochthonous volcano-sedimentary groups have been defined for the Murchison Supergroup in the Murchison Domain based on contact relationships, geochronology, geochemistry, and lithology (Fig. 3). The oldest known components of the Murchison Supergroup lie in the southern part of Murchison Domain, where greenstones in the Golden Grove and Mount Gibson areas have been dated at c. 2960–2945 Ma and c. 2935 Ma, respectively (Yeats et al., 1996; Wang et al., 1998).

At Golden Grove, the c. 2950 Ma succession (>1 km thick) is unconformably overlain by a unit of banded iron-formation and volcanoclastic mass-flow sedimentary rocks that contain zircon populations dated at 2945 ± 4 Ma and 2809 ± 5 Ma (Wang, 1998), the latter of which is interpreted as the age of deposition of this unit. The c. 2810 Ma age of zircons from the younger group of rocks in this area lies within the upper range of the widespread Norie Group (c. 2820–2800 Ma), which forms the lowermost stratigraphic unit across the better exposed and more thoroughly studied northern part of the domain. The Norie Group consists of several kilometres' thickness of stratigraphy commencing with a lowermost interbedded unit of Ti-rich, Al-depleted komatiites and komatiitic volcanoclastic rocks (Barley et al., 2000) and a thick succession of pillowed and massive tholeiitic basalt (Murrouli Basalt; Watkins and Hickman, 1990). Conformably overlying the Murrouli Basalt is the Yaloginda Formation, which consists of rhyolite, fine- to medium-grained felsic volcanoclastic sedimentary rocks, and interbedded units of ferruginous shale and/or banded iron-formation dated at 2814 ± 3 Ma to 2806 ± 4 Ma (Van Kranendonk and Ivanic, 2009). Norie Group volcanism

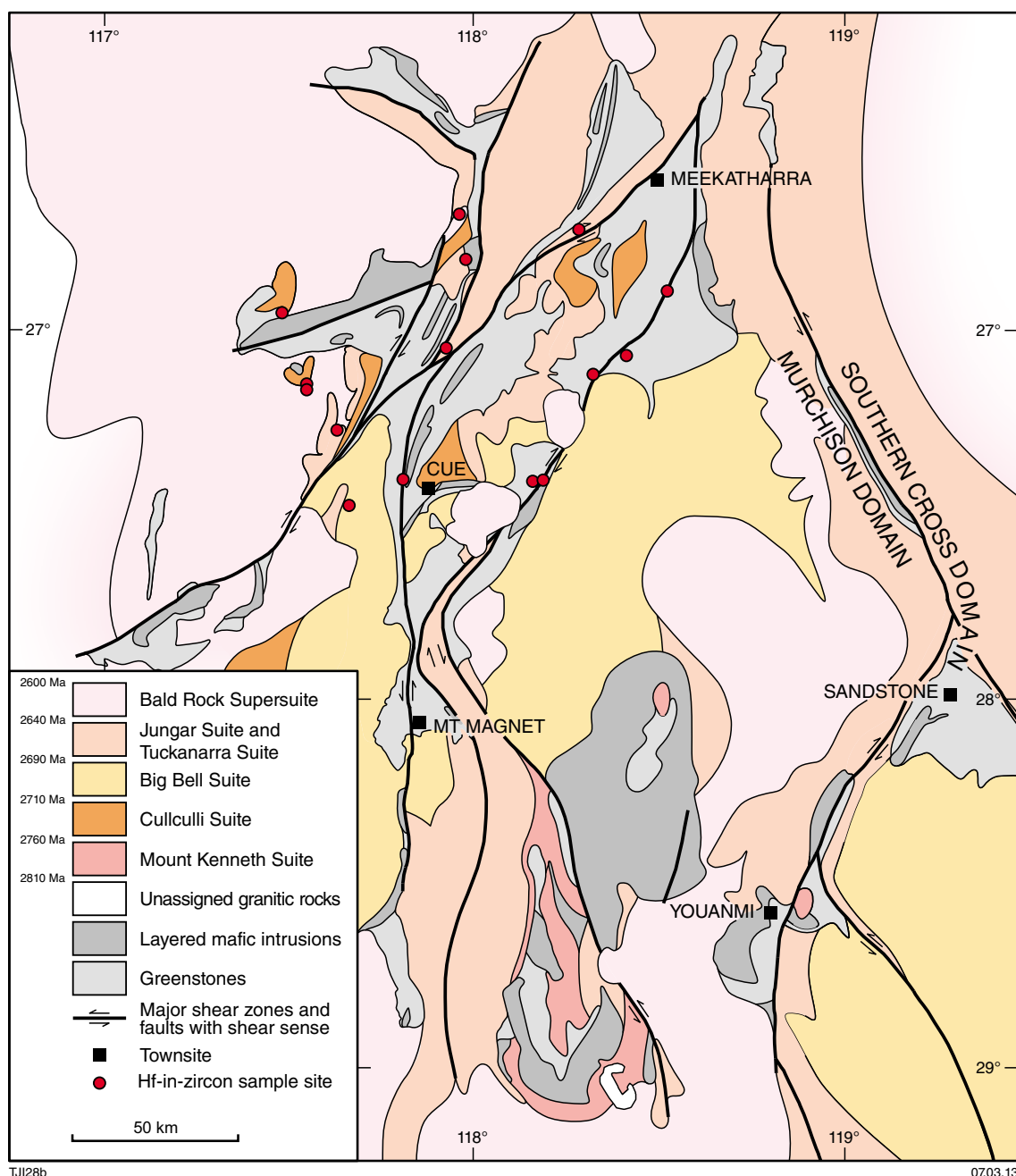


Figure 2. Simplified geological map of the northeastern Murchison Domain, highlighting the locations for Lu–Hf samples and the distribution of granitic suites and supersuites (as red circles). Layered mafic–ultramafic intrusive rocks and greenstones are shaded in grey. Granitic rocks comprise approximately 60% of interpreted bedrock in this area of the Yilgarn Craton, mafic–ultramafic intrusive rocks approximately 20%, and supracrustal greenstone lithologies approximately 20%.

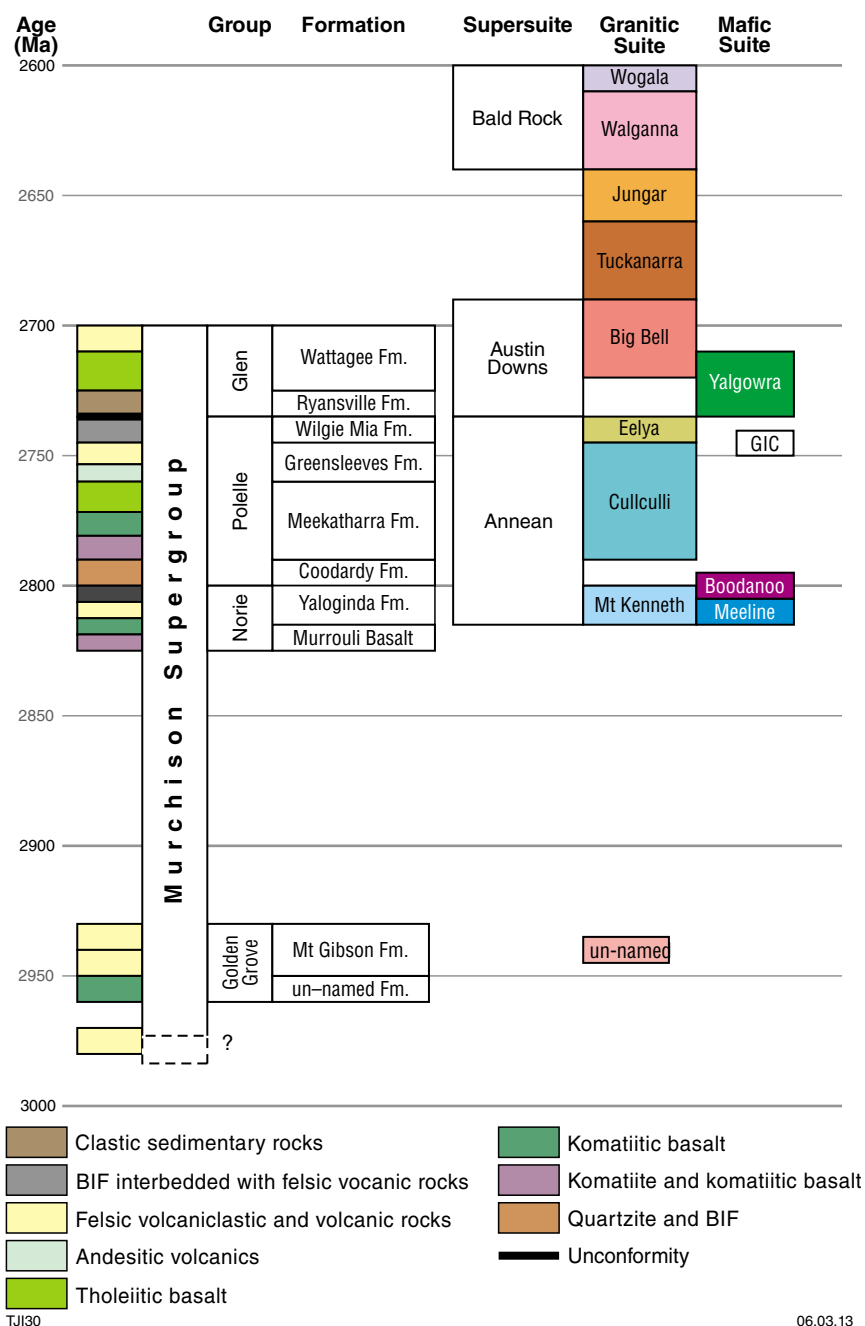


Figure 3. Stratigraphic scheme for the Murchison Domain, divided into two main columns for supracrustal rocks (with generalized lithological column) and intrusive supersuites of granitic suites and mafic-ultramafic suites. Note hiatus in magmatic activity from 2930 to 2820 Ma. The less well studied rocks older than 2900 Ma include dated rocks from an un-named formation and an un-named suite of granites. GIC = Gnanagooragoo Igneous Complex

was accompanied by the emplacement of very large (up to 7 km thick and 80 km diameter), layered mafic–ultramafic igneous complexes of the Meeline Suite (c. 2815 Ma) and Narndee Igneous Complex (c. 2800 Ma; Ivanic et al., 2010).

The c. 2800–2740 Ma Polelle Group conformably overlies the Norie Group. It consists of four conformable formations: (i) the thin, basal quartzitic Coodardy Formation; (ii) the lower Meekatharra Formation of dominantly tholeiitic basalt, komatiitic basalt, komatiite, and thin interflow felsic volcanoclastic sedimentary rocks (c. 2800–2760 Ma); (iii) the intermediate Greensleeves Formation of andesitic to rhyolitic volcanic and volcanoclastic rocks (c. 2760–2740 Ma); and (iv) interbedded banded iron-formation, shale, and felsic volcanoclastic rocks of the Wilgie Mia Formation (c. 2760–2735 Ma). The younger stage of volcanism was accompanied by emplacement of the Gnanagooragoo Igneous Complex ('GIC' in Fig. 3), a thick, differentiated mafic–ultramafic intrusion that was emplaced below and within the banded iron-formations of the Wilgie Mia Formation in the Weld Range at some time between 2752 Ma, the age of plagioclase feldspar crystal tuff unit, and c. 2740 Ma, the age of a crosscutting granitic intrusion (Wang, 1998; Van Kranendonk et al., 2010). The thicknesses of the formations of the Polelle Group are difficult to determine due to deformation; however, they appear to total a minimum of 5 km.

The 2735–2710 Ma Glen Group, which unconformably overlies on the Polelle Group (Van Kranendonk et al., 2010), consists of the lower Ryansville Formation of clastic sedimentary rocks and the conformably overlying Wattagee Formation of komatiitic basalt and subordinate rhyolite. The deposition of the Glen Group was coeval with emplacement of widespread, thick, differentiated gabbro sills of the Yalgowra Suite. As the top contact of the group is not exposed, the thickness of 2 km is a minimum estimate. The cumulative thickness of the Yalgowra Suite sills is approximately 1 km.

Granitic rocks

Following from Van Kranendonk and Ivanic (2009), we observe eight suites of granitic rocks for the northern Murchison Domain based on composition, style and degree of deformation, crosscutting relationships, and age (Figs 2, 3). A ninth, older occurrence of granites has been recorded in the Mount Gibson area in the far southern part of the domain, where 2935 ± 3 Ma monzogranite intrudes the base of greenstones and is contemporaneous with subvolcanic felsic porphyritic intrusions emplaced higher up within the greenstones (Yeats et al., 1996).

In the northern part of the domain, widespread synvolcanic granitic rocks (Annean Supersuite) were emplaced at the same time as the deposition of the Norie and Polelle Groups (c. 2815–2740 Ma). Three geochemically distinct suites have been identified within the supersuite, the oldest being the Mount Kenneth Suite. Plutons from this suite intrude into the upper and marginal regions of large layered mafic–ultramafic igneous complexes of the Meeline and Boodanoo Suites, from c. 2815–2800 Ma,

and are considered to represent local melts generated by the thermal effects of the emplacement of these complexes. Contemporaneous with the Polelle Group, the Cullculli Suite (c. 2785–2735 Ma) is composed dominantly of tonalite–trondhjemite–granodiorite (TTG), which commonly contains a distinctive mafic clotty texture consisting of elliptical (now strained, although originally spherical) hornblende \pm biotite clots from 1 cm to 8 cm in size (Van Kranendonk et al., 2010). Some plutons of the Cullculli Suite also contain synplutonic mafic dykes, while others are mafic tonalite with 15–20% hornblende phenocrysts. The Eelya Suite includes granitic rocks that are particularly enriched in high field strength elements (HFSE; Champion and Cassidy, 2002).

The felsic intrusive rocks of the Austin Downs Supersuite consist of the Big Bell Suite. This supersuite includes foliated tonalitic to monzogranitic rocks ranging in age from c. 2724 to c. 2690 Ma.

The c. 2690–2670 Ma Tuckanarra Suite consists of strongly foliated and locally magmatically layered granodioritic to monzogranitic rocks which intrude greenstone belts, are locally cut by younger K-feldspar monzogranites, and have been affected by the late phase of shear-related deformation (Zibra, 2012). The c. 2665–2640 Ma Jungar Suite consists of foliated to strongly sheared K-feldspar-porphyritic monzogranites, many of which lie within high-strain, ductile strike-slip shear zones.

The post-tectonic Bald Rock Supersuite of undeformed granites is subdivided into two suites: (i) the c. 2630–2610 Ma Walganna Suite of biotite \pm muscovite monzogranite to syenogranite that ranges from coarsely K-feldspar-porphyritic to coarse-grained and equigranular; and (ii) the c. 2605 Ma Wogala Suite of fluorite-bearing alkali granite.

Nomenclature and comparison to previously identified granitic suites

The use of 'supersuite' in this study (also in Van Kranendonk and Ivanic, 2009; Ivanic et al., 2010) is to group several mafic and felsic magmatic 'suites' into distinct pulses of magmatic activity (Fig. 3). That means the Annean Supersuite commences with mafic–ultramafic suites (e.g. Meeline Suite) and associated granitic rocks (Mount Kenneth Suite) and then progresses with the diverse Cullculli and Eelya Suites. The second supersuite, the Austin Downs Supersuite, commences with the intrusion of the Yalgowra Suite and the accompanying Big Bell Suite of granitic rocks. These two supersuites conform to distinct thermo-tectonic events (see Discussion). Finally, the Bald Rock Supersuite encompasses all the 'post-tectonic' granites. This chronological presentation of events was not possible before detailed mapping and geochronology datasets had been acquired. It is not always possible to assign the suite/supersuite of magmatic rocks based on geochemistry alone. Therefore we have relied on a combination of geological field relations, structural observations, geochronology, and geochemistry to assign suite/supersuite where possible (Fig. 3).

Table 1 compares the granitic suites identified here to previous studies. Initial attempts at classification were based primarily on the structural setting (Watkins and Hickman, 1990) and lacked geochronological control. A granitic study in the northern Eastern Goldfield Superterrane and eastern Youanmi Terrane (Champion and Sheraton, 1997) yielded two major and three minor suites. With the absence of the minor ‘syenitic suite’, this system was adopted to account for the range of geochemical compositions of granites in the Murchison Domain (Champion and Cassidy, 2002, 2010). However, detailed mapping, geochronology, geochemistry, and the erection of a new stratigraphic framework (Van Kranendonk and Ivanic, 2009) have led to a more comprehensive series of suites identified here. Table 1 shows that there is a broad equivalence of particular suites of Champion and Cassidy (2002) to the ones presented here. The most direct correlation is between the Eelya Suite and the ‘HFSE suite’, although we identify other examples of the ‘HFSE suite’ within the Jungar, Mount Kenneth, and un-named (c. 2.95 Ga) suites. The ‘mafic suite’ is broadly equivalent to the Cullculli Suite and the ‘high-Ca suite’ is broadly equivalent to parts of the Cullculli, Big Bell, and Tuckanarra Suites. The voluminous ‘low-Ca suite’ is broadly equivalent to the Jungar and Walganna Suites.

Analytical methods

Geochemical data

Major elements were determined at Geoscience Australia (GA) by wavelength-dispersive X-ray fluorescence (XRF) on fused disks using methods similar to those of Norrish and Hutton (1969). Precision is better than $\pm 1\%$ of the reported values and totals range from 99.1 to 100.1 wt%, with all iron as Fe_2O_3 (Appendix, Table A1.1). XRF and trace element concentrations are shown in Table A1.1. Concentrations of Ba, Cr, Ni, Sc, V, Zn, and Zr were determined by wavelength-dispersive XRF on pressed pellets using methods similar to those of Norrish and Chappell (1977), whereas Cs, Ga, Nb, Pb, Rb, Sr, Ta, Th, U, Y, and the rare earth elements were analysed by inductively coupled plasma – mass spectrometry (ICP-

MS; Agilent 7500 instrument) using methods similar to those of Eggins et al. (1997), on solutions obtained by dissolution of fused glass disks (Pyke, 2000). Precision for trace elements is better than $\pm 10\%$ of the reported values. Samples 81740, 81760, 81770, 169003, and 169067 are legacy data obtained from <<http://geochem.doir.wa.gov.au/geochem/>> and were analysed more than 10 years ago, so these data are potentially less reliable. However, major elements fall into the range 98.6 – 100.8 wt% (all iron as Fe_2O_3 , Table A1.1).

Isotopic data

Hafnium isotope analyses of previously dated zircon grains mounted in epoxy resin were conducted using a New Wave/Merchantek LUV213 laser-ablation microprobe attached to a Nu Plasma multi-collector inductively coupled plasma mass spectrometer (LA-MC-ICP-MS). The analyses used a beam diameter of approximately 55 μm and a repetition rate of 5 Hz, which produced typical ablation pits 40–60 μm deep. The ablated sample was transported from the laser cell to the ICP-MS torch by helium carrier gas. Interference of ^{176}Lu on ^{176}Hf was corrected by measurement of interference-free ^{175}Lu , and using the invariant $^{176}\text{Lu}/^{175}\text{Lu}$ correction factor 1/40.02669 (DeBievre and Taylor, 1993). Interference of ^{176}Yb on ^{176}Hf was corrected by measuring the interference-free ^{172}Yb isotope, and using the $^{176}\text{Yb}/^{172}\text{Yb}$ ratio to obtain the interference-free $^{176}\text{Yb}/^{177}\text{Hf}$ ratio. The appropriate value of $^{176}\text{Yb}/^{172}\text{Yb}$ was determined through spiking the JMC475 hafnium standard solution with Yb, and finding the value of $^{176}\text{Yb}/^{172}\text{Yb}$ (0.58669) required to yield the $^{176}\text{Hf}/^{177}\text{Hf}$ value for the unspiked solution.

Fourteen zircon grains from the Mud Tank carbonatite locality were analysed, together with the samples, as a monitor of the accuracy of the results. All of the data and the mean $^{176}\text{Hf}/^{177}\text{Hf}$ value (0.282523 ± 0.000011 ; $n = 14$) are within two standard deviations of the recommended value of 0.282522 ± 0.000042 (2σ) (Griffin et al., 2007). Two analyses of the 91500 zircon standard analysed during this study indicated $^{176}\text{Hf}/^{177}\text{Hf} = 0.282315 \pm 0.000024$ (2σ), which is within uncertainty of the accepted value (Goolaerts et al., 2004; Griffin et al., 2006).

Table 1. Classifications of granitic suites from this study compared with those in previous studies

<i>Approximate age range (Ma)</i>	<i>Granitic suite (this study)</i>	<i>Watkins and Hickman (1990) scheme</i>	<i>Champion and Cassidy (2002) scheme</i>
2950–2920	Un-named	Pegmatite banded gneiss	High-Ca / Mafic / High-HFSE
2815–2800	Mount Kenneth	–	High-Ca / Mafic/ High-HFSE
2785–2735	Cullculli	Post-folding Suite 1, 2	Mafic / High-Ca
2750–2735	Eelya	Post-folding Suite 1, 2	High-HFSE
2720–2690	Big Bell	Post-folding Suite 1, 2	High-Ca
2690–2670	Tuckanarra	Recrystallized monzogranite/pegmatite banded gneiss	High-Ca (minor Low-Ca)
2665–2640	Jungar	Recrystallized monzogranite/pegmatite banded gneiss	Low-Ca / High-Ca / High-HFSE
2640–2610	Walganna	Recrystallized monzogranite	Low-Ca
2610–2600	Wogala	–	Low-Ca

Lu–Hf analyses of previously dated zircon crystals characterizes the isotopic ratio of the source region(s) from which the magma evolved, which may enable a distinction between grains that have formed at the same time although with different ratios of crustal and mantle contributions. The measured $^{176}\text{Lu}/^{177}\text{Hf}$ ratios of the zircons have been used to calculate initial $^{176}\text{Hf}/^{177}\text{Hf}$ ratios. Initial $^{176}\text{Hf}/^{177}\text{Hf}$ values are calculated using the decay constant of Scherer et al. (2001) and calculation of ϵHf values used the chondritic values of Blichert-Toft and Albarède (1997). Depleted mantle model ages (T_{DM}^c) were calculated using the measured $^{176}\text{Lu}/^{177}\text{Hf}$ ratios, referred to a model depleted mantle with present-day $^{176}\text{Hf}/^{177}\text{Hf}$ ratio of 0.28325 (Nowell et al., 1998) and $^{176}\text{Lu}/^{177}\text{Hf}$ ratio of 0.0384 (Griffin et al., 2000). Crustal model ages, assuming derivation from a depleted mantle (T_{DM}^c) were calculated for the source of the magma using the initial $^{176}\text{Hf}/^{177}\text{Hf}$ ratio of the zircon and assuming a mean crustal value of $^{176}\text{Lu}/^{177}\text{Hf} = 0.015$ (Griffin et al., 2002) for the store of Hf after extraction from the mantle but prior to incorporation in the zircon crystal lattice. Hf isotopic results for all samples used in this study are shown in Table A1.2 and are presented in Figure 4b on an initial $^{176}\text{Hf}/^{177}\text{Hf}$ evolution plot. All 88 analyses are from zircons with <10% discordant U–Pb systematics.

Lu–Hf isotopic data are filtered using the calculated alpha dose for each U–Pb spot based on the U and Th concentrations and $^{207}\text{Pb}/^{206}\text{Pb}$ age (Murakami et al., 1991). Calculated alpha doses corresponding to a metamict state are indicated in Table A1.1. Metamict grains are classified as those having $>8 \times 10^{15}$ alpha events per milligram and such grains are excluded from further consideration (Murakami et al., 1991). This screening method has also been applied to the detrital zircon populations within selected samples of Griffin et al. (2004).

Results

Lu–Hf and U–Pb data

Table A1.2, in Appendix 1 ‘Analytical results and geochemical model’, summarizes the Lu–Hf and U–Pb analytical data.

Summary of samples with Lu–Hf and U–Pb data

178102

Sample 178102 is a hornblende-bearing tonalite from Finger Post Bore (Wingate et al., 2008a), which intrudes greenstones of Norie Group. Twenty-nine analyses of twenty-nine euhedral, idiomorphically zoned zircon crystals yield a weighted mean $^{207}\text{Pb}^*/^{206}\text{Pb}^*$ date of 2787 ± 3 Ma (mean square of the weighted deviates, MSWD = 1.28), which is interpreted as the age of magmatic crystallization (Wingate et al., 2008a). ϵHf values for nine analyses of these grains are greater than chondritic uniform reservoir (CHUR) (0.10 to 3.63) and correspond to a mean T_{DM}^c of 3.1 Ga.

178103

Sample 178103 is a metamonzogranite approximately 20 km southwest of Meekatharra and belongs to the Jungar Suite of metagranitic rocks. Zircons from this sample are mainly subhedral to euhedral and up to 300 μm long. Concentric growth zoning is ubiquitous. Nineteen analyses were obtained from 19 zircons. The date of 2655 ± 5 Ma for 17 analyses is interpreted as the age of magmatic crystallization of the granite (Wingate et al., 2008b). ϵHf values straddle CHUR (1.41 to -3.00) and correspond to a mean T_{DM}^c of 3.2 Ga.

178105

Sample 178105 is an andesite from Woolgra Bore (Wingate et al., 2008c). The andesite is part of Woolgra Andesite Member of the Greensleeves Formation, Polelle Group, located in the core of the Polelle Syncline. It is interpreted to overlie mafic volcanic rocks of the Meekatharra Formation. Eighteen analyses of 18 subhedral to euhedral, idiomorphically zoned zircons yield a weighted mean $^{207}\text{Pb}^*/^{206}\text{Pb}^*$ date of 2755 ± 5 Ma (MSWD = 1.32), interpreted as the age of igneous crystallization of the andesite (Wingate et al., 2008c). ϵHf values for six analyses of these grains are greater than CHUR (0.63 to 3.85) and correspond to a mean T_{DM}^c of 3.2 Ga.

178141

Sample 178141 is a quartz diorite from the Callisto mine and is assigned to the Cullculli Suite intrusive rocks into the Polelle Group (Van Kranendonk and Ivanic, 2009). Ten analyses of euhedral elongate zircons yield a weighted mean $^{207}\text{Pb}^*/^{206}\text{Pb}^*$ date of 2746 ± 5 Ma (MSWD = 3.1), interpreted as the magmatic crystallization age (Wingate et al., 2009a). ϵHf values from six analyses range from near CHUR to more evolved (-4.08 to 0.66). T_{DM}^c model ages range from 3.0 to 3.2 Ga.

178142

Sample 178142 is a flow-banded to massive rhyolite from close to Mount Cullculli. The rhyolite is assigned to the Yaloginda Formation of the Norie Group, Murchison Supergroup. Zircon crystals from this rock are stubby prisms up to 200 μm long that display idiomorphic zoning under cathodoluminescence (CL). Eighteen analyses of 18 zircon crystals yield a weighted mean $^{207}\text{Pb}^*/^{206}\text{Pb}^*$ date of 2806 ± 4 Ma (MSWD = 1.3), which is interpreted as the age of igneous crystallization (Wingate et al., 2011a). ϵHf values for six analyses of these grains are near CHUR (-0.04 to 1.30) and correspond to a mean T_{DM}^c of 3.2 Ga.

178194

Sample 178194 is a granite orthogneiss from the Coodardy Homestead that is assigned to the Annean Supersuite of metamorphosed felsic and mafic intrusive rocks, which occur within the Polelle Group (Van Kranendonk and Ivanic, 2009). Twelve analyses of 12 zircons with idiomorphic zoning yield a weighted mean $^{207}\text{Pb}^*/^{206}\text{Pb}^*$ date of 2744 ± 3 Ma (MSWD = 1.09), interpreted as the age of magmatic crystallization (Wingate and Van Kranendonk,

2009). One inherited grain yields a $^{207}\text{Pb}^*/^{206}\text{Pb}^*$ date of 2958 ± 5 Ma. ϵHf values, from six analyses of 2750 Ma magmatic zircon, are more evolved than CHUR (-6.72 to -1.52), averaging -2.8 , with T_{DM}^{c} model ages averaging 3.4 Ga. The single inherited grain yields a ϵHf value of 0.87 and a T_{DM}^{c} model age of 3.3 Ga.

178196

Sample 178196 is a monzogranite containing mafic clots from west of Glen Station. The monzogranite is assigned to the Annean Supersuite, which intrudes the Polelle Group of the Murchison Supergroup. Eighteen analyses of 18 zircon grains with faint oscillatory zoning yield a weighted mean date of 2748 ± 2 Ma (MSWD = 0.63) (Wingate et al., 2011c). Two grains yield older dates of 2908 ± 8 Ma and 2925 ± 16 Ma and are interpreted to represent material inherited from either the source or wallrock of the intrusion. ϵHf values for seven analyses of the c. 2750 Ma magmatic grains show a considerable range, spanning from more radiogenic than CHUR to more evolved (-10.05 to 2.44), with a median around -4 . T_{DM}^{c} model ages range between 2.9 to 3.4 Ga. One inherited grain analysed yields a ϵHf value of -0.77 and a T_{DM}^{c} model age of 3.4 Ga.

178197

Sample 178197 is a medium-grained biotite monzogranite from 5 km west of Glen Station. The monzogranite is part of the Walganna Suite of the Bald Rock Supersuite. Zircon crystals are mainly subhedral to euhedral, and up to 300 μm long, with concentric growth zoning ubiquitous. Twelve analyses were obtained from 12 zircons and a date of 2623 ± 9 Ma for a cluster of 11 analyses is interpreted as the age of magmatic crystallization of the monzogranite (Wingate et al., 2009b). A wide range of extremely negative ϵHf values was obtained from these zircons, from -5.6 to -12.78 , corresponding to a range of T_{DM}^{c} from 3.46 to 3.84 Ga.

178199

Sample 178199 is a foliated granodiorite assigned to the 2686–2665 Ma Tuckanarra Suite of metamorphosed granodioritic to monzogranitic rocks (Van Kranendonk and Ivanic, 2009), which occurs within the Meekatharra – Mount Magnet greenstone belt. Seventeen analyses of 16 zircons with faint indications of oscillatory zoning form a single age component, with a weighted mean $^{207}\text{Pb}^*/^{206}\text{Pb}^*$ date of 2675 ± 3 Ma (MSWD = 0.81), interpreted as the age of magmatic crystallization of the granodiorite (Wingate et al., 2009c). ϵHf values from nine analyses range from -3.46 to 0.97, although they predominantly cluster around CHUR. T_{DM}^{c} model ages average 3.2 Ga.

185922

Sample 185922 is a leucogabbro sill from Fleece Pool and is assigned to the Yalgowra Suite, Austin Downs Supersuite (Van Kranendonk and Ivanic, 2009; Ivanic et al., 2010). Twelve analyses of 11 zircons and zircon fragments with euhedral concentric growth zoning yield a weighted mean $^{207}\text{Pb}^*/^{206}\text{Pb}^*$ date of 2735 ± 5 Ma,

interpreted as the igneous crystallization age of the gabbro sill (Wingate et al., 2010b). ϵHf values from eight analyses are predominantly more evolved than CHUR (-8.48 to 0.50). T_{DM}^{c} model ages range between 3.0 and 3.5 Ga.

185923

Sample 185923 is a hornblende–biotite–quartz diorite from 450 m south of Walga Rock Road. This rock is assigned to the Cullculli Suite, Annean Supersuite (Van Kranendonk and Ivanic, 2009). Sixteen analyses of 16 zircons with idiomorphic zoning yield a weighted mean $^{207}\text{Pb}^*/^{206}\text{Pb}^*$ date of 2724 ± 2 Ma (MSWD = 1.07), interpreted as the magmatic crystallization of the diorite (Wingate et al., 2011d). ϵHf values from six analyses are near CHUR (-0.83 to 1.78) with T_{DM}^{c} model ages that average 3.2 Ga.

185927

Sample 185927 is a leucogabbro sill from Barloweerinyer Hill and has been assigned to the Waladah Gabbro of the Yalgowra Suite (Van Kranendonk and Ivanic, 2009; Ivanic et al., 2010). Thirty analyses of crystals with weakly developed euhedral growth zoning yield a weighted mean $^{207}\text{Pb}^*/^{206}\text{Pb}^*$ date of 2711 ± 2 Ma (MSWD = 0.99), interpreted as the age of magmatic crystallization (Wingate et al., 2010a). ϵHf values from nine analyses range from -1.08 to 1.62 and T_{DM}^{c} model ages average 3.2 Ga.

185929

Sample 185929 is a medium to coarse-grained biotite muscovite fluorite granite from 2 km north of Wogala Bore. The granite is assigned to the Wogala Suite of the Bald Rock Supersuite. Zircons are subhedral to euhedral, equant to elongate, and concentric growth zoning is ubiquitous. Fourteen analyses were obtained from 14 zircons and the date of 2606 ± 5 Ma for 13 analyses is interpreted as a magmatic crystallization age of the granodiorite (Wingate et al., 2011b). A wide range of extremely negative ϵHf values was obtained from these zircons, from -4.6 to -10.3 , corresponding to a range of T_{DM}^{c} from 3.41 to 3.77 Ga.

185932

Sample 185932 is a monzogranite from 7 km west of Robin Outcamp Well. The monzogranite is assigned to the 2785–2735 Ma Cullculli Suite, Annean Supersuite, which intrudes the Polelle Group of the Murchison Supergroup. Fourteen analyses of 14 zircons yield a concordia age of 2746 ± 4 Ma (MSWD = 0.71), interpreted as the age of magmatic crystallization (Wingate et al., 2012a). ϵHf values for six analyses range from slightly more radiogenic than CHUR to evolved (-3.70 to 1.06). T_{DM}^{c} model ages range between 3.0 and 3.2 Ga.

185933

Sample 185933 is a biotite granodiorite from Eelya North Mine (Wingate et al., 2010c). The granodiorite is assigned to the 2760–2735 Ma Eelya Suite of the

Annean Supersuite, which intrudes the Polelle Group of the Murchison Supergroup (Van Kranendonk and Ivanic, 2009). Thirty-three analyses of idiomorphically zoned crystals yields a weighted mean $^{207}\text{Pb}^*/^{206}\text{Pb}^*$ date of 2759 ± 2 Ma (MSWD = 1.3), interpreted as the age of magmatic crystallization (Wingate et al., 2010c). εHf values for eight analyses of these grains range from near CHUR to more evolved values (−1.28 to 0.97). T_{DM}^{c} model ages cluster at 3.2 Ga.

193972

Sample 193972 is a rhyolite clast from a felsic volcanic breccia 5 km west of the Madoonga Homestead. The breccia is part of the Wilgie Mia Formation of the c. 2800–2730 Ma Polelle Group, although the sample represents a clast that was situated within, and is therefore older than, the breccia. Zircons isolated from this sample are up to 200 μm long, and equant to slightly elongate; concentric zoning is ubiquitous. Eighteen analyses were obtained from 18 zircons. The date of 2979 ± 3 Ma for the 14 analyses is interpreted as the magmatic crystallization age of the rhyolite from which the clast was derived (Wingate et al., 2012b). A wide range of εHf values was obtained from these zircons, from 1.97 to −3.55, corresponding to a range of T_{DM}^{c} from 3.25 to 3.65 Ga.

Whole-rock geochemical data

Whole-rock geochemical data for granitic rocks are tabulated in Table A1.1 and are plotted on primitive mantle (PM) – normalized rare earth element (REE) and trace element diagrams in Figures 5 and 6, respectively. Figure 7 shows selected divariant plots for individual elements and ratios.

Annean Supersuite

Granitic rocks of the c. 2815–2735 Ma Annean Supersuite show a range of geochemical characteristics indicating derivation from, and possibly interaction between, different sources. Two samples from the c. 2815–2800 Ma Mount Kenneth Suite (191037, 193987) that intrude into the Windimurra Igneous Complex have 74.2–75.8 wt% SiO_2 and 0.24–5.2 wt% MgO, respectively. High silica and high Y in these samples is compatible with high degrees of fractionation, whereas high MgO and moderate Ni in 193987 indicates at least some contamination by mafic material. Rocks from this suite have flat and elevated REE patterns, with significant, though variable, negative Eu anomalies (Fig. 5a). The flat profile forms a so-called birdwing pattern (Schaltegger and Kr henb hl, 1990), which is characteristic of highly fractionated felsic magmas, as also indicated by high Y and heavy REE (HREE) (Figs 7f and 5a, respectively). Alternatively, these patterns are consistent with high-temperature partial melting of tholeiitic rocks. The rare earth element pattern is similar to the contemporaneous (2813 ± 3 Ma) Kantie Murdannia Volcanics Member (dashed line, Fig. 5a, 169003) and other related felsic volcanic rocks of this age (e.g. 169067, Fig. 5a), which are found above the roofs of the igneous complexes of the Meeline and Boodanoo Suites. Granites of the Mount Kenneth Suite lie on a low

Sr vs SiO_2 trend (Fig. 7b), indicative of generation at low pressures (Moyen et al., 2009).

The Cullculli Suite of hornblende-bearing tonalites and dioritic rocks (samples 190934, 190541, 81760, 186928, 178141, and 185923) has low SiO_2 (62–67 wt%) and K_2O (average 2.8 wt%), and high MgO (average 2.4 wt%). These are the most mafic and least evolved granitic rocks identified in the Murchison Domain, in terms of high MgO and low SiO_2 (Fig. 7c). In terms of their REE patterns (black lines on Fig. 5b), the rocks from this suite show distinctly ‘spoon-shaped’ patterns, which have higher LuN/YbN (typically >1) and lack Eu anomalies, which distinguishes them from other rocks in the supersuite. These rocks also show lesser Nb, Ta, and Sr anomalies (Figs 5b, 6a). Figure 7a shows how this suite has a range of Sr/Zr ratios within a wider range of Annean Supersuite rocks. This could indicate a variety of sources contributing to the formation of these rocks. La vs Th and Nb vs Y also show wide spreads for this suite in particular (plots not shown). The ‘spoon-shaped’ HREE profiles for the Cullculli Suite, and elevated LuN/YbN, indicate generation by melting of amphibolite under relatively high-pressure conditions (Martin et al., 2005). Such conditions are also suggested by typically absent Eu and Sr anomalies and elevated Sr vs SiO_2 (Fig. 7b).

Remaining granitic rocks of the Annean Supersuite (several of which have overlapping ages with those of the Cullculli Suite – 178194, 185920, 185921, 178104, and 178196) show higher SiO_2 (68–74 wt%) and K_2O (average 3.9 wt%), and lower MgO (average 0.65 wt%). Rare earth element patterns remain negatively sloped into the HREE and they typically show negative Eu anomalies (Fig. 5b). Nb and Sr anomalies are larger than for Cullculli Suite rocks (Fig. 6a). These show the widest range of Sr/Zr ratios (Fig. 7a) and likely encompass diverse types of melting and possibly varying sources. Low and high Sr trends may indicate generation at variable pressures.

A mixing origin for the Cullculli Suite is also permissible at least in part. Figure 8 and Table A1.3 illustrate a simple binary mixing of 25 and 50% of an average Meekatharra Formation basalt with a typical Annean Supersuite metagranite (178194), which produces distinctly similar REE patterns to these Cullculli Suite rocks. (Sample 178141 of quartz diorite is shown for comparison in Table A1.3 and Fig. 8.) In addition, a very close match is produced in terms of major and other trace elements with a few exceptions: (i) the Cullculli Suite has some very high Th, Ce, and La samples; (ii) the Cullculli Suite has higher MgO, Nb, and HREE; and (iii) unreasonable quantities (>50%) of Meekatharra Formation basalt would be required to explain the full range of some of the trace elements such as Ba and light rare earth elements (LREE).

We account for (i) with minor alteration of mobile elements in these typically greenschist facies rocks. It is difficult to account for (ii); however, it is possible that the initial felsic melt might have been slightly higher in Nb and HREE. In addition the initial basaltic melt might have been slightly more evolved, which would elevate the modelled compositions of these elements. Local fractionation of olivine and chromite may account for

discrepancies in MgO, Ni, and Cr concentrations in the modelling. The most difficult to account for is (iii) since it is mechanically difficult to mix homogeneously in a 50–50 ratio. Therefore, if mixing were a major factor in the formation of the Cullculli Suite, it would likely be at a lower ratio and involve slightly different starting compositions, which we failed to sample at the surface.

Additional evidence such as common and widespread clotty mafic texture in many Cullculli Suite granites (Van Kranendonk et al., 2010, fig. 32) suggests incomplete mixing of coeval felsic and mafic magmas. Variable amounts of magma mixing and variable degrees of hornblende fractionation in the mid–lower crustal source would therefore account for the vast majority of the range of major and trace element compositions found in the Cullculli Suite. Significant fractionation of other minerals alone (e.g. garnet) is unable to create Cullculli Suite-like rare earth element patterns. Without involvement of a higher MgO and lower large ion lithophile element (LILE), and LREE mafic component, major and trace elements cannot be matched.

The coeval felsic magmas may be generated by using existing or new underplated material. Here, the felsic component may have resulted from the fractionation of melts of a pyroxenitic/eclogitic underplate derived from previous plume-related magmatism, rather than being the direct results of in situ fractionation of juvenile melts.

The Peter Well Granodiorite of the Eelya Suite (185933) is unique in having elevated ($10 \times$ PM) and flat HREE, and a large negative Eu anomaly (Fig. 5b). This rock has elevated Nb, Y, and Zr compared to other Annean Supersuite rocks (Fig. 6a). These features are typical of felsic magmas with elevated HFSE signatures as also found in some Greensleeves Formation felsic volcanic rocks. These rocks include the ‘high-HFSE group’ from Champion and Cassidy (2002).

Big Bell Suite

Only a single sample of monzogranite has been analysed (including one duplicate analysis) from the Big Bell Suite. It has moderate SiO₂ (71.5 wt%), low MgO (0.5 wt%), and rare earth element patterns similar to the Cullculli Suite, lacking a Eu anomaly, and with a spoon-shaped rare earth element profile (Fig. 5c).

Jungar and Tuckanarra Suites

The post-volcanic Jungar and Tuckanarra Suites consist primarily of metamonzogranites. Geochemical data from these suites show that post-volcanic rocks are typically more potassic and silicic than synvolcanic granitic rocks. Compared with the synvolcanic Cullculli Suite granites, most Jungar Suite and Tuckanarra Suite granites (except 178199) have steeper REE profiles ($(\text{La}/\text{Yb})_N = 22.4\text{--}83.0$) and significant negative Eu anomalies ($(\text{Eu}/\text{Eu}^*)_N = 0.29\text{--}0.68$) (Fig. 5d). The younger (2665–2640 Ma) Jungar Suite granites have typically more fractionated rare earth element profiles, with steeper slopes, than those of the older (2690–2665 Ma) Tuckanarra Suite. Figure 6b shows that Jungar Suite rocks

are elevated in LILE (e.g. Cs, Rb, Ba) and LREE, and Figure 5d shows that they also have more significant Eu anomalies than the Tuckanarra Suite.

The samples of the Tuckanarra Suite with high Na₂O (4.5 – 7 wt%) and low CaO (0.9 – 1.5 wt%) and Y have very similar REE profiles to some Annean Supersuite granites (Figs 5b, d), indicating a similar source for these rocks through melting of amphibolite at deep crustal levels. However, all rocks from this suite preserve significant Eu anomalies (Fig. 7d) and lesser Nb anomalies (Fig. 7e), indicating derivation from shallower crustal levels than the Cullculli Suite. This is also apparent from Figure 7b, where these suites lie at intermediate Sr and SiO₂ when compared to the other granitic suites. Moderately negative Ba anomalies (i.e. suggestive of moderate feldspar fractionation in the source) are also indicative of moderate depths of formation for these suites (Fig. 6b). Figure 7a shows that the Jungar Suite rocks form along the most variable array of Sr/Zr ratios (La/Th and Nb/Y are also variable in this suite; plots not shown). Therefore, it is likely that several compositions of basement rocks in the middle crust melted to produce the Jungar Suite.

Bald Rock Supersuite

The post-tectonic granites of the Bald Rock Supersuite have characteristically high SiO₂ and low MgO (Fig. 7c) and the largest negative Eu anomalies ($(\text{Eu}/\text{Eu}^*)_N = 0.07\text{--}0.37$, Figs 5e, f, 7d) of all analysed, dated granites. The two samples of the Walganna Suite have shallow rare earth element slopes and elevated HREE ($(\text{La}/\text{Yb})_N = 3.5\text{--}18.6$), characteristic of moderately fractionated I-type granites (Fig. 5e). The fluorite-bearing granites from the Wogala Suite (c. 2606 Ma) have a birdwing-shaped rare earth element pattern with depleted medium rare earth element (MREE) levels at elevated concentrations of $10\text{--}20 \times$ PM (Fig. 5f), suggestive of extremely fractionated granitic rocks involving the fractionation, in particular, of titanite (Schaltegger and Krähenbühl, 1990). Both suites show extremely elevated Cs, Rb, and Th (Fig. 6c). Sr vs SiO₂ composition is indicative of a low-pressure genesis for this suite (Fig. 7b; Moya et al., 2009).

From c. 2750 Ma during intrusion of the Cullculli Suite, through to the end of the time of emplacement of the Jungar Suite, granitic rocks become progressively more and more fractionated. The 2640–2600 Ma Bald Rock Supersuite is the most fractionated, having the highest Y (and other incompatible element) values (Fig. 7f). Low Sr and high SiO₂ (Fig. 7b) and highly negative Ba anomalies (Fig. 6c) indicate derivation from relatively shallow crustal depths involving extensive fractionation of feldspars. Figures 5e and 5f indicate that the post-tectonic granites evolved through time from the Walganna Suite to the Wogala Suite. These rare earth element patterns reveal their derivation through progressive fractionation through time from a progressively evolving crustal source.

Overall, early granitic components (2750–2670 Ma) show relatively shallow REE profiles with small negative Eu anomalies ($(\text{La}/\text{Yb})_N = 9.4\text{--}30.4$, $(\text{Eu}/\text{Eu}^*)_N = 0.46\text{--}0.77$, Fig. 7d). Progressively younger granites to

c. 2645 Ma have increasingly higher SiO_2 and higher LREE concentrations (25 to $200 \times \text{PM}$). From c. 2645–2600 Ma, the rare earth element patterns of granites changes and shows lower LREE concentrations (from 200 to $20 \times \text{PM}$) and higher SiO_2 . Significantly, all post-volcanic granites show a progressive increase in HREE and increasingly more negative Eu anomalies (to $(\text{Eu}/\text{Eu}^*)_N = 0.08 - 0.2$) from c. 2710–2600 Ma. These data document the geochemical variations involved in the cratonization process and they suggest that the lower crust would have evolved through progressive melt depletion.

Lu–Hf isotope data

Lu–Hf isotope analyses were performed on zircons from 16 samples that had been previously dated by the U–Pb SHRIMP method (Table A1.2). These samples include a variety of lithologies representing the whole range of Murchison Domain evolution. Of these, four samples are of felsic volcanic rocks, two are of c. 2735–2711 Ma gabbros of the Yalgowra Suite (185922, 185927), and the rest are granites. Felsic volcanic rocks analysed include one sample of a c. 2806 Ma flow-banded rhyolite (178142) of the Yaloginda Formation (Norie Group), and andesite (Woolgra Andesite Member, 178105) and rhyolite (185923) from the Greensleeves Formation (Polelle Group). One sample containing c. 2980 Ma zircons from a rhyolite clast within a c. 2750 Ma felsic volcanoclastic rock from the Wilgie Mia Formation has also been analysed for Lu–Hf isotopes. Granitic rocks include a c. 2787 Ma hornblende tonalite (Cullculi Suite, 178102), four granitic rocks of the Annean Supersuite (hornblende tonalite, 178141; granitic orthogneiss, 178194; clotty hornblende tonalite, 178196; Eelya Suite, 185933), foliated hornblende quartz diorite of the Big Bell Suite (185923), foliated monzogranite of the Tuckanarra Suite (178199), and two post-tectonic Bald Rock Supersuite granites (178197, 185929).

The results of Lu–Hf isotope analysis of dated zircons from these samples indicate a dramatic change in the age of source regions for melts emplaced into the Murchison Domain over the period c. 2980–2600 Ma (Figs 4a, b). The oldest components analysed at c. 2980 Ma have a moderately juvenile source with ϵHf values of 0 ± 3 (Fig. 4a). The ancient sources required for these samples highlight the possibility that the lower crustal basement rocks may be closely related to older Narryer Terrane material. Alternatively, the tectonic interleaving of Narryer Terrane and Murchison Domain rocks at depth is possible (Myers, 1995). For the following approximately 110 m.y., from c. 2930–2820 Ma, there is a hiatus in zircon crystallization events. Then, from c. 2810–2755 Ma, this hiatus is followed by crystallization of zircons which have ϵHf values from 0 to +3 (Fig. 4a) and clearly show derivation from a relatively juvenile source (T_{DM} 3.04 Ga, Fig. 4b), consistent with derivation from dominantly mafic–ultramafic nature of magmatism at this time. This is also consistent with geochemical evidence of derivation of associated felsic volcanic rocks through high degrees of fractionation of tholeiitic magma chambers or by partial melting of tholeiitic rocks, possibly including underplated material. The Lu–Hf data

array from younger rocks shows that the juvenile 3.04 Ga source component is apparent throughout the subsequent evolution of the Murchison Domain (Fig. 4b).

At c. 2760 Ma, there is a sharp change to include a much older (unradiogenic) source region during the generation of andesitic to rhyolitic volcanic rocks of the Greensleeves Formation and granitic rocks of the Annean Supersuite. ϵHf model ages indicate that this older source is c. 3.80 Ga, much older than any rocks preserved at the surface and of a similar age to those of the Narryer Terrane to the northwest (i.e. 3.65–3.73 Ga). It is possible that the Narryer Terrane docked with the Youanmi Terrane at this time (Nutman et al., 1993); however, our data suggest that this older material is beneath the northwest Youanmi Terrane and not, as previous authors suggested, thrust over. Further evidence is that rocks of this age could be present lower down in Murchison Domain crust, as indicated by evidence from inherited zircon xenocrysts (Nelson et al., 2000).

From c. 2720 to c. 2640 Ma, the older source does not appear to be involved in the generation of melts emplaced at the level of present surface erosion. This suggests that an older source region that contributed to the generation of older melts was not involved in the generation of these younger melts sampled in this study. Rather, it was isolated somewhere within the crust, possibly at lower levels. This is despite the fact that granitic melts continued to evolve to more fractionated compositions across this entire interval. However, Lu–Hf data from detrital zircons (Griffin et al., 2004) does show that this ancient 3.80 Ga (possibly Narryer Terrane material) source is involved continuously from c. 2760 Ma through to c. 2600 Ma. The detrital zircons may have been transported from other terranes in the Yilgarn Craton; therefore, this feature cannot be assumed for the Murchison Domain until further analysis is undertaken.

At c. 2640 Ma, there was again a sharp change in the age of the source region for granitic plutons emplaced at the level of the present erosional surface. As with the older volcanic rocks of the Greensleeves Formation and granitic rocks of the Annean Supersuite, post-tectonic plutons of the Murchison Domain were derived from melting of an older source (which ϵHf T_{DM} model ages indicate is up to approximately 3.80 Ga). The array of data from c. 2640–2600 Ma is evolved in comparison to the rest of the data as it lacks an abundance of CHUR-like and positive ϵHf values. Therefore a juvenile source is not required for the generation of the Bald Rock Supersuite. However, the array of Hf data is likely generated by mixing with a more juvenile component aged between 3.0 and 2.7 Ga.

Of the two samples of zircons from Yalgowra Suite gabbros sills (185922, 185927), sample 185922 yields CHUR-like values at c. 2.72 Ga. As these zircons crystallized in the contact zone of the gabbro sills, they likely experienced crustal contamination and are not expected to reflect the juvenile, probably depleted, mantle isotopic characteristics of the gabbro melt source. In sample 185927, a xenocrystic nature of some zircons may account for negative ϵHf values.

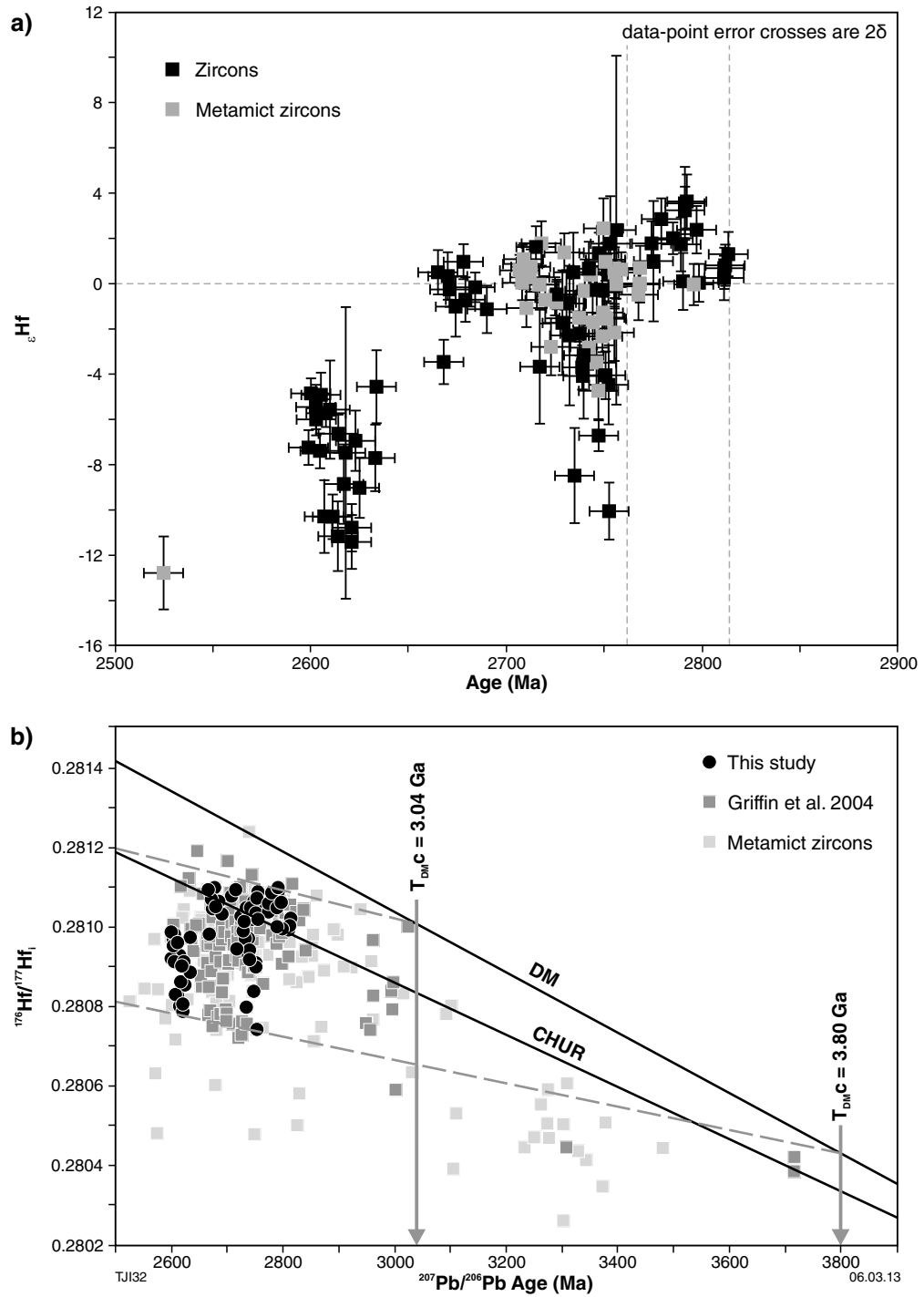


Figure 4. a) ϵ_{Hf} vs ^{207}Pb – ^{206}Pb age (Ma) plot for zircons from the northern Murchison Domain samples in this study (see also Ivanic et al., 2012). Black squares indicate crystalline zircons and grey squares indicate high-alpha dosage metamict grains (see Appendix 1, Table A1.2). 2σ error bars are shown. Vertical dashed lines highlight juvenile compositions from c. 2815 Ma to c. 2770 Ma; b) $^{176}\text{Hf}/^{177}\text{Hf}_i$ vs Pb–Pb age (Ma) for data from this study (black circles), Griffin et al. (2004) detrital zircons (dark grey squares), and metamict grains from both this study and Griffin et al. (2004) data shown as light grey squares. Depleted mantle (DM) and chondritic uniform reservoir (CHUR) evolution lines are shown for reference. Two vertical dashed lines indicate the period of solely juvenile activity from 2810 to 2755 Ma. Dashed lines indicating the maximum and minimum depleted mantle model ages (T_{DMC}) in Ga for the data from crystalline zircons in this study are also shown using a $^{176}\text{Lu}/^{177}\text{Hf}$ ratio of 0.015 (Griffin et al., 2004); see text for discussion.

Discussion

Previous work

Previous studies of the Yilgarn Craton have led to contrasting tectonic models. On the one hand, plume models of crust formation have been advocated for the whole craton (Campbell and Hill, 1988). On the other, variations of arc-accretion models have also been proposed for the whole of the Yilgarn Craton (Myers, 1995) or, more specifically, for the Eastern Goldfields Superterrane (Morris and Witt, 1997; Barley et al., 2008; Kositsin et al., 2008; Czarnota et al., 2010).

The petrogenesis for the four groups of granites previously identified in the Murchison Domain (Champion and Cassidy, 2002) is summarized as follows:

1. 'High-Ca group', derived from mafic (LILE-poor) source and either produced by melting a subducted slab or by deep melting within a thickened crust
2. 'Low-Ca group', derived from a high LILE, high-HFSE source and produced by remelting of continental crust
3. 'High-HFSE group' derived at intermediate pressures from an intermediate SiO_2 crustal source or from fractionation of mafic melts
4. 'Mafic group' derived from crustal and mantle components, possibly by subduction-fluid metasomatism of the mantle source.

This study delineates a progressive evolution of granitic rocks in relation to the stratigraphic development of the Murchison Domain over 200 m.y. The petrogenetic interpretations presented here are derived independently, although they are compatible with those identified by Champion and Cassidy (2002). For example, we interpret many of the granites of the 'Low-Ca group' to be remelted crust as evidenced by Hf isotopes and we interpret the many of the granites of the 'High-Ca group' to be deep melts within a thickened crust.

The main difference in the interpretations of the granitic suits is with the Cullulli Suite, which overlaps considerably with the 'mafic group' of Champion and Cassidy (2002). We interpret these granites to be the result of mafic-felsic magma mixing, rather than a subduction-modified source. We base this on the mafic-clotty textures we observe in the field and initial success in modelling mixed compositions of likely sources (Figure 8).

Griffin et al. (2004) analysed detrital zircons from the northern Yilgarn Craton (Fig. 4b) to generate a broad pattern of Lu-Hf isotope evolution through time for this area. They inferred an ancient >3.4 Ga crustal component that was recycled in younger magmas within the 'Murchison Province' (now the Murchison Domain). They also inferred that a 3.2 Ga depleted-mantle source contributed significantly to magmatism in the Murchison Domain from 2.9 to 2.6 Ga. We also removed significant scatter from a large proportion of metamict detrital zircons in this dataset (see 'Analytical methods') to highlight

meaningful data trends in relation to the data gathered here from in situ magmatic zircons (Fig. 4b). Our data provide tighter constraints on the model ages for Murchison Domain rocks and hence clearer evidence as to the ages of older crust-forming events. Overall, good correspondence is seen between the new data in this paper and the detrital zircon data. The filtered detrital zircon data of Griffin et al. (2004) show two juvenile grains at c. 3.70 Ga, which are probably associated with the c. 3.80 Ga juvenile event, highlighted as the oldest component tapped in samples from this study. However, no rocks of this age have been identified at the surface in the northern Murchison Domain. The detrital data also delineates a crustal evolution trend back to a c. 3.04 Ga (and possibly slightly younger) juvenile event. Additionally, four to five detrital grains with the most negative ϵHf values (below the lower dashed line in Fig. 4b) indicate that the oldest material incorporated into Murchison Domain magmas might be as old as c. 4.00 Ga. However, the older detrital zircons may be derived from granitic rocks outside the study area, with sources like those that yielded the Eoarchean and Hadean detrital zircons in quartzite in the Southern Cross Domain to the east as described in Wyche (2007). Lu-Hf data from zircons from the Southern Cross Domain and Eastern Goldfields Superterrane (Fig. 1; Wyche et al., 2012) reveal a similar pattern to that of Griffin et al. (2004). However, the oldest component is not seen in the Eastern Goldfields samples (Wyche et al., 2012).

Recent studies in the northern Murchison Domain have proposed variations on plume models to account for the sequence of voluminous mafic-ultramafic magmatic events observed (Van Kranendonk and Ivanic, 2009; Ivanic et al., 2010). Following the major plume event that produced the Norie Group and early components of the Annean Supersuite, widespread crustal melting of several source regions is considered to have been responsible for the deposition of the thickest group, the Polelle Group, between c. 2790 and c. 2735 Ma. The final phase of greenstone development, the Glen Group, is related to uplift and erosion between c. 2735 and c. 2710 Ma during extension accompanied by further input of mantle melts into the crust (Ivanic et al. 2010). Recent geochronological evidence from the large mafic-ultramafic igneous complexes of the Murchison Domain has also provided spatial and temporal constraints on significant additions of juvenile material to the crust. Ivanic et al. (2010) suggested that an ancient rift zone in the central Youanmi Terrane may have been a focus for the mafic-ultramafic magmatism at c. 2800 Ma, caused by a mantle plume.

Sm-Nd model-age data from granites in the Murchison Domain have indicated that there is a broad, northeasterly trending corridor of rocks between Meekatharra and Mount Magnet (Fig. 2) with younger depleted mantle model ages (T_{DM}) to 2.95 Ga, compared with adjacent parts of the domain that have T_{DM} ages to 3.3 Ga (Champion and Cassidy, 2002; Ivanic et al., 2010). This concept is certainly compatible with data presented in this study.

Interpretation of geochemical data

The geochemical data presented in this Report, when combined with new lithostratigraphic, isotopic, and U-Pb

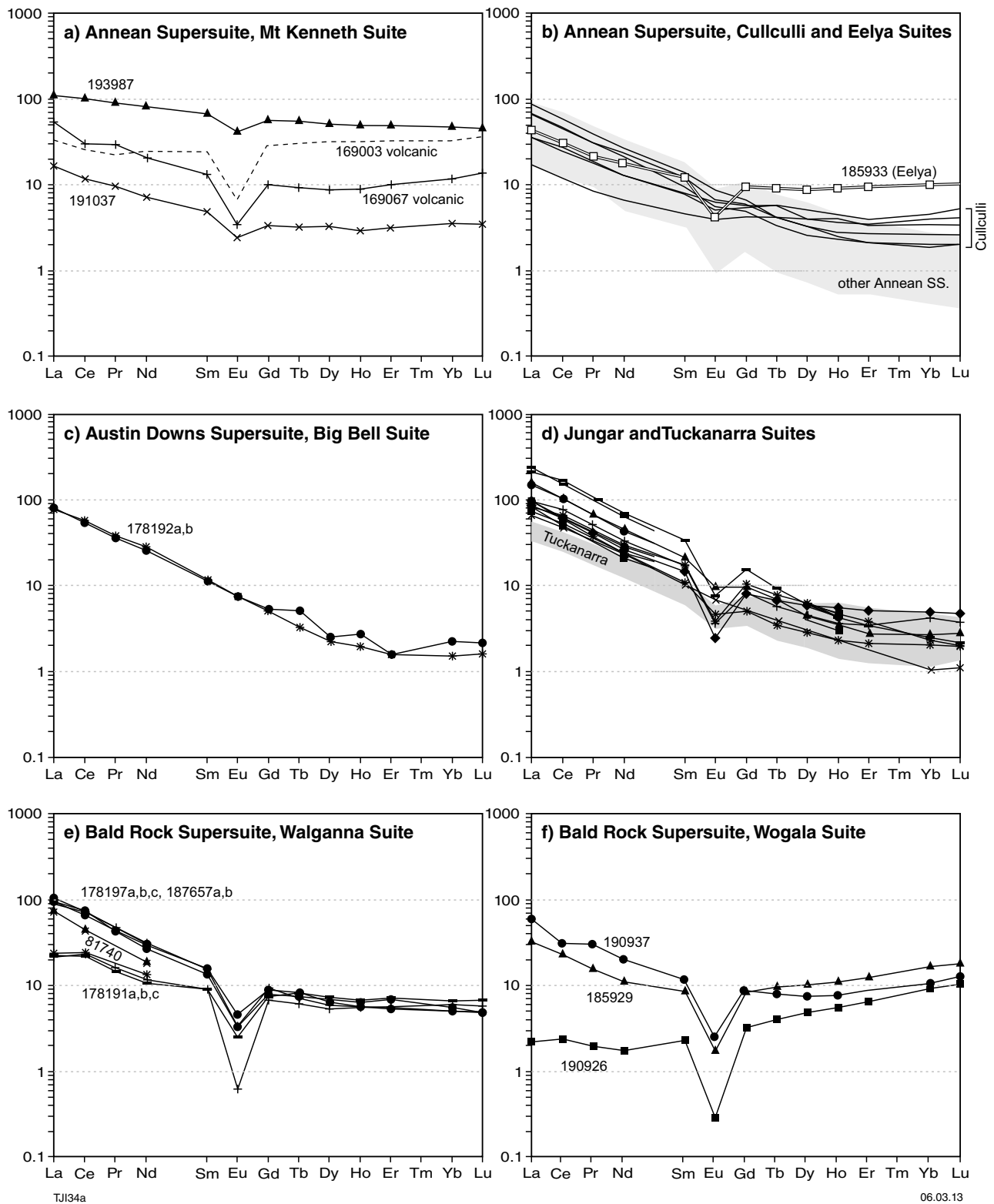


Figure 5. Primitive mantle (PM)-normalized rare earth element plots (using PM values from Sun and McDonough, 1989) for the granitic suites of the northern Murchison Domain. a) Mount Kenneth Suite (193987, 191037), showing the composition of a coeval rhyolite from the Kantie Murchidana Volcanics (169003, dashed line) and coeval felsic volcanic from Pincher Well (169067); b) Cullculli Suite (black lines) compared to other Annean Supersuite metagranitic rocks (grey area). The single Eelya Suite sample (185933) is shown as a line with white square symbols; c) Big Bell Suite, duplicate analyses of a single sample 178192; d) Tuckanarra Suite (shaded grey area) and Jungar Suite (black lines); e) Walganna Suite; f) Wogala Suite. PM normalization is used for direct comparison with Figure 6 since these samples do not have any subchondritic values.

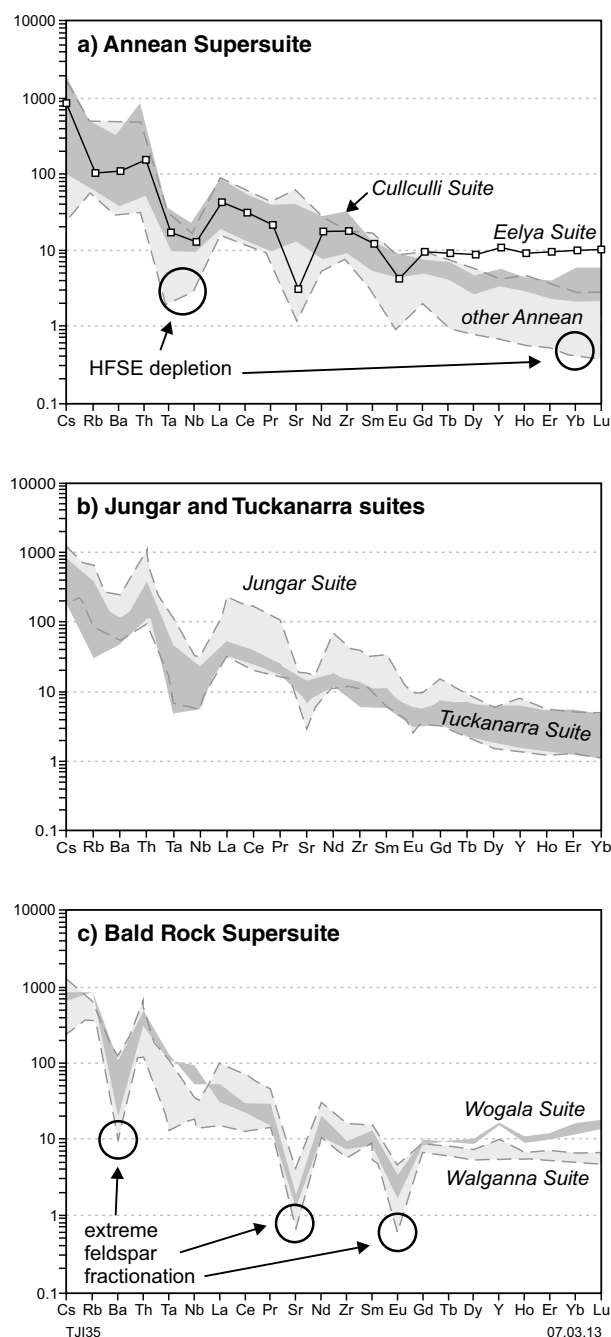


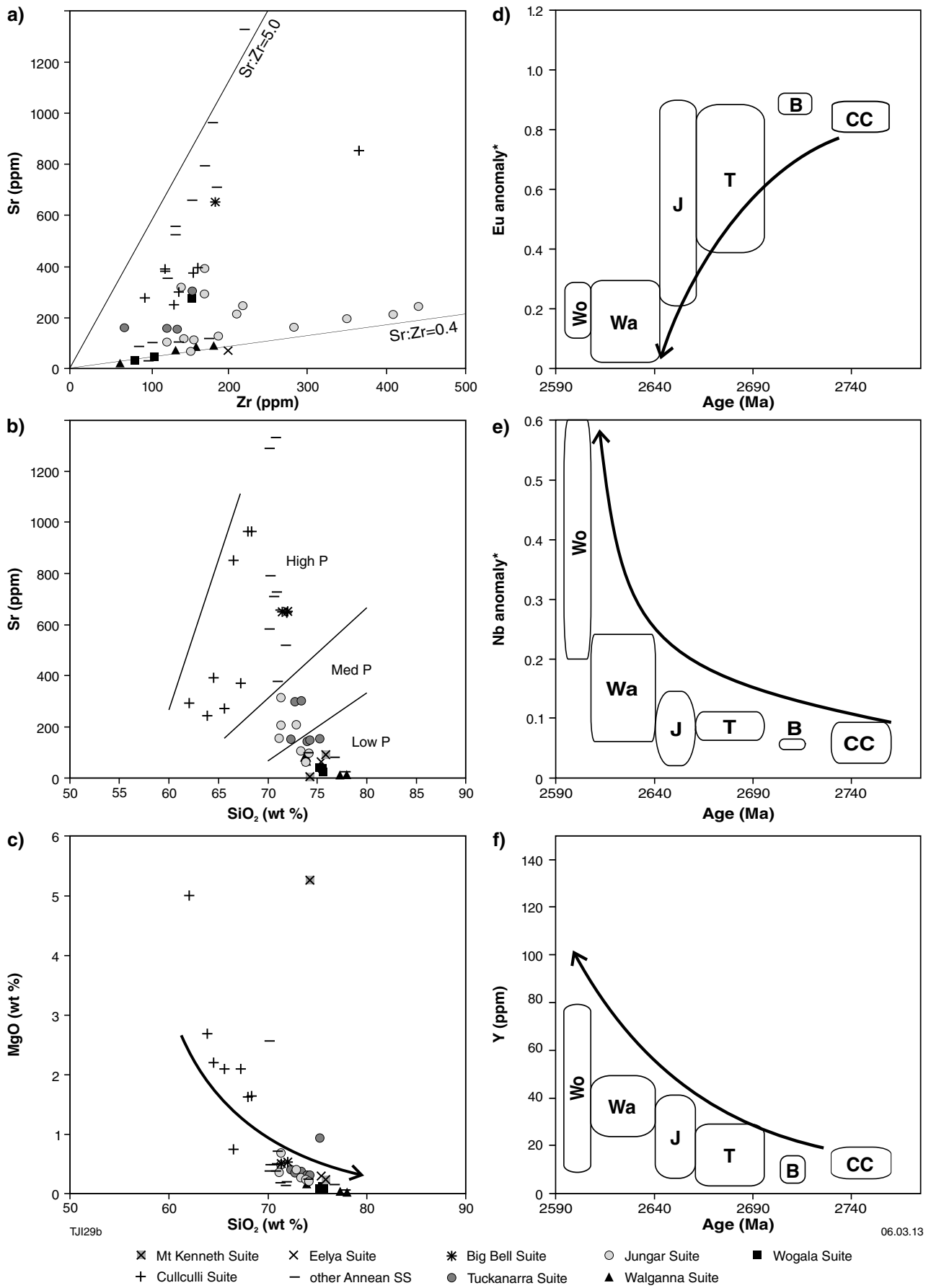
Figure 6. Primitive mantle-normalized trace element diagrams (using values of PM from Sun and McDonough, 1989) for selected granitic suites and supersuites of the northern Murchison Domain: a) Cullculli Suite (dark shaded grey area) compared to other Annean Supersuite rocks (light shaded grey area with dashed grey outline) and the Eelya Suite sample (solid black line with white square symbols); b) Jungar and Tuckanarra Suites, with the Jungar Suite shown as a light grey area (dashed outline) and the Tuckanarra Suite shown as a darker grey area; c) Bald Rock Supersuite with the Walganna Suite shown as a light grey area (dashed outline) and the Wogala Suite shown as a darker grey area.

geochronological data, show that crustal development of the Murchison Domain was essentially continuous for 225 m.y., from c. 2825 to c. 2600 Ma, and superimposed on an earlier period of crustal development at c. 2980 Ma. The two events were separated by a hiatus in magmatic activity of approximately 110 m.y., which is represented in the field by an angular unconformity (Van Kranendonk et al., 2010).

The c. 2815–2800 Ma Mount Kenneth Suite of granites shows characteristic geochemical indications for highly fractionated shallow melts, contaminated by coeval mafic magmatism. It is also possible that they represent melts of tholeiitic rocks. These granites are only spatially associated with large layered mafic–ultramafic intrusions and are considered part of the same magmatic event. Contemporaneous felsic volcanic successions (e.g. the Kantie Murdanna Volcanics; Nelson, 2001) adjacent to, and overlying, the granitic and mafic–ultramafic intrusive rocks have trace element compositions compatible with those of the Mount Kenneth Suite (Fig. 5a). Therefore, the volcanic rocks are also considered to be genetically related to the intrusion of the voluminous Meeline and Boodanoo Suites (Ivanic et al., 2010).

After c. 2800 Ma, a relatively continuous evolution trend in the compositions of granitic rocks commenced with the Cullculli Suite, which is the least fractionated of all granitic suites in the Murchison Domain. Ba, Sr, Eu, and HREE data suggest that rocks of this suite are derived from melting of amphibolite (\pm an older crustal component) within the lower crust. Field data and a variety of MgO compositions indicate that a significant mixing of mantle-derived mafic material and crustal material is also required to form these rocks. Multiple sources are supported by wide scatter on Sr vs Zr (Fig. 7a), Nb vs Y, and Th vs La plots. Various degrees of fractionation of hornblende in the source can account for the range of HREE compositions of this suite. The contemporaneous Eelya Suite shows HFSE enrichment and is interpreted to be a local fractionate derived from similar sources to the Cullculli Suite. The c. 2720–2690 Ma Big Bell Suite shows many similar features to the Cullculli Suite. These rocks were assigned to the ‘mafic group’ (Champion and Cassidy, 2002), and although interpreted as deep melts of mafic lower crust, it was noted that they could have an origin of a metasomatized mantle source, as identified for other sanukitoid-like rocks.

The trend towards shallower and more evolved melts recommences with the high K₂O and moderately to strongly fractionated REE granites of the Tuckanarra and Jungar Suites, respectively. Previous investigations ascribed such granites to either small volume melts or a source with only minor amphibole, at moderate crustal levels (Champion and Cassidy, 2002). Geochemical data presented here indicate derivation from intermediate depths in the crust with moderate to strong fractionation, with the Jungar Suite likely derived from shallower levels than the Tuckanarra Suite. These suites can be interpreted as being derived primarily from partial melting of pre-existing granitic crust, with a smaller component derived from anhydrous partial melting of a tonalitic source in the lower crust (e.g. sample 178199), probably driven by



06.03.13

Figure 7. (facing) Trace element plots for the granitic suites of the northern Murchison Domain: a) Sr vs Zr with lines indicating the range of Sr/Zr ratios in the datasets; b) Sr vs SiO₂ (wt%) with lines dividing low, medium, and high-pressure regions (after Moyen et al., 2009); c) MgO vs SiO₂ (wt%) with an arrow indicating a generalized intermediate-to-evolved trend for the data; d) Eu anomaly* (= $\text{Eu}/0.5 \times (\text{Sm} + \text{Gd})/\text{N}$) vs age (Ma) with areas outlining the chemical variations within the granitic suites described. Arrow indicates the general increase in negative Eu anomaly from c. 2750 to c. 2600 Ma. Wo = Wogala Suite, Wa = Walganna Suite, J = Jungar Suite, T = Tuckanarra Suite, B = Big Bell Suite, CC = Cullculli Suite; e) Nb anomaly* (= $\text{Nb}/0.5 \times (\text{Th} + \text{La})/\text{N}$) vs age (Ma) with areas outlining the chemical variations within the granitic suites described. Arrow indicating the general decrease in negative Nb anomaly from c. 2750 to c. 2600 Ma. Abbreviations as for d); f) Y (ppm) vs age (Ma) with areas outlining the chemical variations within the granitic suites described. Arrow indicates the general increase in Y abundance from c. 2750 to c. 2600 Ma. Abbreviations as for d), and duplicate analyses are shown for 178101–4, 178190–9, 187640–65, and 190525.

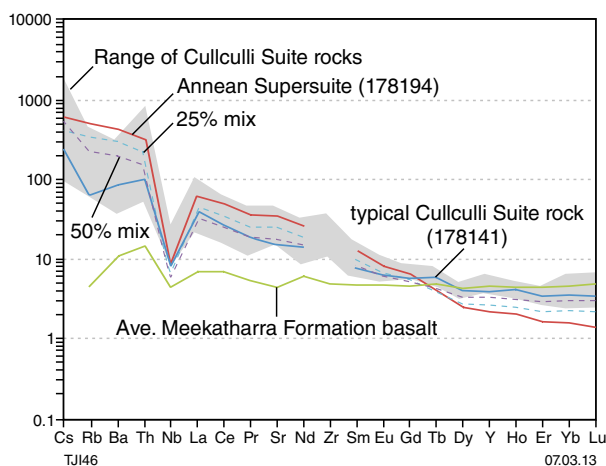


Figure 8. Trace element compositions for the result of mixing Meekatharra Formation basalt and Annean Supersuite granodiorite in relation to the composition of the Cullculli Suite tonalitic rocks.

biotite breakdown. The Jungar Suite shows highly variable Sr/Zr ratios, which could indicate diverse source rocks for this suite.

The final phase of granitic magmatism in the Yilgarn Craton, the Bald Rock Supersuite, continues the trend towards shallower and more highly fractionated rocks. Features such as birdwing rare earth element patterns, large negative Eu anomalies, and enrichment of LREE and HFSE indicate derivation from high-temperature partial melting of a middle-crustal, intermediate to more siliceous source (Champion and Cassidy, 2002).

Between c. 2750 Ma and c. 2600 Ma, granitic rocks typically become more silicic and potassic, and less

aluminous and calcic. This is likely due to successive remelting of granitic crust at progressively shallower crustal levels, producing progressively more fractionated granitic rocks to develop a depleted, and hence residual, lower crust during cratonization.

Interpretation of Lu–Hf isotope data

In the northern Murchison Domain, the oldest zircons analysed for Lu–Hf isotopes are from a single detrital sample (193872) dated at c. 2980 Ma. The array of ϵ_{Hf} values (Fig. 4a) for this sample ranges up to +2, which is considered evidence that the older history of greenstone development in the domain involved the addition of juvenile material into older crust. The spread of data down to ϵ_{Hf} –4 signifies that these magmas incorporated some Paleoproterozoic material and involved mixing of a juvenile and a more evolved component to generate this vertical array (Fig. 4b). This array is the first indication of crustal reworking in Murchison Domain felsic rocks. This also indicates the possible involvement of Narryer Terrane-aged material (Kinny et al., 1988) as basement to the older Murchison Domain supracrustal rocks. Further investigation is required in more extensive regions of c. 2950 Ma rocks in the southern Murchison Domain to delineate this array to its full extent.

We consider one (non-metamict) zircon grain at 3.04 Ga (Fig. 4b; Griffin et al., 2004) to have crystallized directly from a juvenile mantle (either lithospheric or asthenospheric) source, which appears to represent a crust-forming event of the domain. The array generated for northern Murchison Domain zircons could represent successive tapping of this source (upper dashed projection line, Fig. 4b) and variable degrees of mixing with considerably more evolved crustal components. The most evolved of these samples project back to approximately 3.80 Ga (lower dashed projection line, Fig. 4b). In our dataset we do not directly sample uncontaminated mantle source material from c. 2.81 and 2.72 Ga mantle melting events, which are recognized within the region (Ivanic et al. 2010). Zircon grains from gabbros in the Yalgowra Suite are from a marginal zone and may be crustally contaminated. The upper bound to the zircon Hf array implies continued sampling of a 3.04 Ga source; nevertheless additional juvenile input events and their mixture with unradiogenic crust could also account for this array. A combination of these processes is reasonable.

In more detail, the Lu–Hf data are consistent with the geochemical data in showing that Murchison Domain crust evolved from a situation with significant juvenile addition of mantle-derived material at c. 2820–2760 Ma including tapping a 3.04 Ga source component. This then evolved to a situation of dominantly in situ, infracrustal differentiation (i.e. reworking of the 3.04 Ga source) and reworking an older 3.80 Ga (possibly Narryer Terrane material) source component thereafter (Fig. 9). This second phase (post-2760 Ma) documents continued juvenile input until c. 2640 Ma. Given the evidence for development of this entire succession on a basement of yet older crust (c. 2.95 Ga and possibly older), the data are consistent with Neoproterozoic crustal development of Murchison Domain as the result of long-lived activity of

mantle plume(s). Close in time to the recommencement of magmatism and juvenile input at c. 2.81 Ga, the Meeline and Boodanoo Suites, which contain V and minor Cu–Ni–platinum group element mineralization and are among the world's largest layered mafic–ultramafic igneous complexes, were emplaced into the crust at this time. This is consistent with impingement of a mantle plume during this time (Fig. 9; Ivanic et al. 2010) and consistent with moderately positive ϵ_{Hf} values from 2820 to 2760 Ma. This is also consistent with our interpretation that granitic rocks of the Mount Kenneth Suite and other crustal materials of this age are derived from tholeiitic sources (see 'Interpretation of geochemical data' section).

The first significant departure from positive ϵ_{Hf} values in these data occurs for zircons of the Greensleeves Formation and Annean Supersuite granites, coinciding with a change from dominantly mafic–ultramafic magmatism to intermediate and felsic magmatism in Murchison Domain history, at c. 2760–2720 Ma. The major addition of low ϵ_{Hf} compositions may be related to the melting of a much older (c. 3.80 Ga) source deeper in the crust. The melts generated during this period were derived from a wide variety of sources. These sources include deep- and medium-crustal amphibolites (sources for TTGs), lower to middle crust (source for high-HFSE granites and felsic volcanic rocks), and (during the latter stages at c. 2720 Ma) primitive mantle melts and highly fractionated tholeiitic magmas (the source for felsic volcanic rocks). Mixing of magmas derived from mantle and crustal melting is seen in clotty mafic granites of the Cullculli Suite and is our preferred interpretation for the generation of this portion of the Hf isotopic array (Fig. 9). This interpretation differs from the typical interpretation of sanukitoid-like granitic rocks in the Archean as subduction-related melts (De Oliveira et al., 2010).

The sharp onset and timing of the switch from dominantly mafic–ultramafic magmatism to andesitic and rhyolitic volcanism at c. 2760 Ma is intriguing. We know that mafic–ultramafic magmatism in the northern Murchison Domain was long lived and continued from c. 2820 Ma to at least c. 2790 Ma. The timing of intrusion of the first synvolcanic granites at c. 2790 Ma is 30 m.y. after the onset of deep, plume-derived ultramafic–mafic volcanism and is compatible with derivation through crustal melting as a result of conductive heat from the plume (Campbell and Hill, 1988). The c. 2760 Ma onset of widespread granitic magmatism corresponds with a time lag of 30 m.y. after the end of major, mantle-derived magmatism and, given the broad range of source regions indicated by the geochemical data and the evidence of highly negative ϵ_{Hf} isotope compositions at this time, it is possible that the switch to intermediate–silicic magmatism was due to widespread crustal melting and mixing between waning mantle magmatism and more voluminous crustal melts produced in response to prolonged conductive heating of older lower crust (Fig. 9).

An alternative interpretation for the sudden departure from solely juvenile input at c. 2760 Ma is that there was a change in tectonics from plume-derived magmatism to the onset of subduction zone magmatism. Indeed, Andean-style volcanism, and hence, subduction-related

tectonic settings, have been suggested for andesitic–rhyolitic volcanic rocks in the adjacent Southern Cross Domain (c. 2735 Ma; Taylor and Hallberg, 1977), as well as for c. 2690 Ma in the Kurnalpi Terrane of the Eastern Goldfields Superterrane (Morris and Witt, 1997; Barley et al., 2008). However, Archean andesites are known to show significant compositional differences with Phanerozoic counterparts (Pearce, 2008) and andesitic rocks can form outside active subduction zones (Willbold et al., 2009).

The komatiitic–tholeiitic basalt composition of the c. 2720 Ma Glen Group and c. 2735–2710 Ma Yalgowra Suite shows that new mantle-derived melts were emplaced into the Murchison Domain at this time. This is supported by the relatively juvenile Lu–Hf composition of zircons aged between 2720–2700 Ma (Fig. 4a) and suggests a renewed period of crust formation through mantle-derived processes. This may be related to the impingement of a second mantle plume, which most likely facilitated the widespread generation of granitic magmas thereafter.

The timing of this event is very similar to the c. 2705 Ma regional komatiite event in the Kalgoorlie Terrane of the Eastern Goldfields Superterrane (Kositcin et al., 2008). In the model of Campbell and Hill (1988), this is inferred to represent a plume event, followed by intracrustal differentiation, producing vast volumes of granitic rocks. Therefore, it is conceivable that this juvenile event in the Murchison Domain at c. 2720 Ma is the same event as documented in the EGST and the second plume event to affect the region. The first proposed plume event at c. 2810 Ma (Ivanic et al., 2010), produced vast intrusive igneous complexes (e.g. Windimurra Igneous Complex, Meeline Suite), and was followed by Polelle Group mafic–ultramafic volcanism (c. 2800–2770 Ma). This is compatible with modelled time ranges of approximately 20–30 m.y. for these thermal events (Campbell and Griffiths, 1990), followed by a period of conductive heat transfer vertically through the crust over approximately 50 m.y. This period of heat transfer may be responsible for the granitic magmatic activity from c. 2770–2720 Ma.

The c. 2690–2630 Ma Tuckanarra and Jungar Suite granites have ϵ_{Hf} values that are close to CHUR ($\epsilon_{\text{Hf}} \approx 0$), although they lie along an array indicative of the continued involvement of the 3.04 Ga source (Figs 4b, 9b). Zircons crystallizing during intrusion of the subsequent Bald Rock Supersuite also have significantly negative ϵ_{Hf} , although they lack CHUR-like values, indicating continued remelting of the older crustal sources between c. 2665 Ma and c. 2600 Ma. In this case, it is highly unlikely that this reflects a subduction processes because of the widespread intrusion of these low-Ca granites across most of the Yilgarn Craton (Champion and Cassidy, 2002). A linear belt of magmatism would be expected for any arc–subduction scenario. For these suites, it is also noted that they occur during a previously proposed 'hiatus' or time of reduced magmatic activity from 2680 to 2655 Ma (Champion and Cassidy, 2002). As these are voluminous suites, we suggest downplaying this hiatus. Figure 2 shows that the Big Bell, Tuckanarra, and Jungar Suites account for the bulk of granitic magmatism in the northern Murchison Domain and hence the timing for a crustal overturn event (if it occurred) would be 2710–2640 Ma.

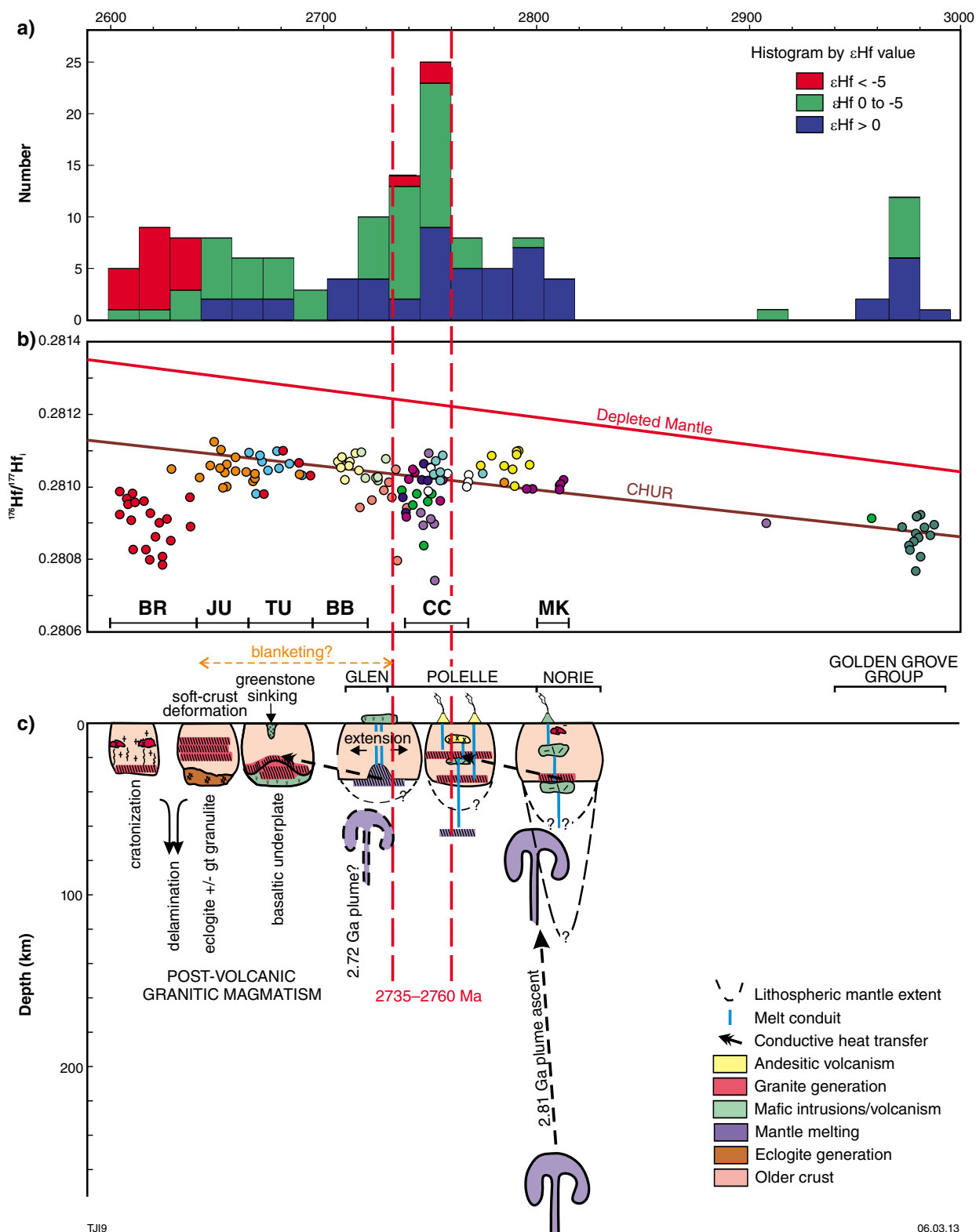


Figure 9. Summary tectonic evolution diagram: a) Histogram of ϵ_{Hf} vs age (Ma). Red bars indicate periods of coeval radiogenic and unradiogenic sources; b) $^{176}\text{Hf}/^{177}\text{Hf}_i$ vs age in Ma (axis at top of part a) for data from this study (samples are shown with single unique colours); depleted mantle and chondritic uniform reservoir (CHUR) evolution model lines shown for reference. Selected suites and supersuites shown at bottom of diagram for reference (BR = Bald Rock Supersuite, JU = Jungar Suite, TU = Tuckanarra Suite, BB = Big Bell Suite, CC = Cullculli Suite, MK = Mount Kenneth Suite); c) Tectonic evolution illustrated with six diagrammatic cross-sections through the lithosphere (and asthenosphere) (age axis at top of part a). Deep melting (>200 km, Barley et al., 2000) is indicated in the deep-sourced 2.81 Ga plume and the possibility of a second plume is shown at c. 2.72 Ga. The significant departure of ϵ_{Hf} to extremely negative values (< -5) is highlighted by vertical dashed red lines across the whole diagram (2760 and 2735 Ma) and shown to overlap with the onset of diverse melt sources found during deposition of the Polelle Group.

The switch to more evolved sources post-2.65 Ga has previously been identified in the Sm–Nd isotope system (Champion and Cassidy, 2002). This observation was also linked to a shallowing of depth of melting during this time. This means the source for these later granites shallowed from a deeper, less evolved, more mafic lower crust to a more evolved middle crust, which is consistent with our interpretation (Fig. 9c).

Implications for Archean granite genesis

The Murchison Domain contains a remarkable record of continuous, although geochemically progressively evolving, granite magmatism over c. 210 m.y., from the oldest synvolcanic granites at c. 2810 Ma to the youngest post-tectonic granites at c. 2600 Ma. The earliest granites in this succession (c. 2810–2800 Ma) are shallow crustal melts associated with adjacent and contemporaneous layered mafic–ultramafic igneous complexes of vast size. This event is identified as the major phase of juvenile input into the crust and interpreted to be the result of the impingement of a mantle plume into the base of the lithosphere, which also tapped a 3.04 Ga mantle source. The involvement of 3.04 Ga source material (i.e. basement material of Golden Grove Group age) was important from 2810–2650 Ma (Fig. 9b) and the involvement of older basement in the source was significant at least at c. 2750 Ma and c. 2620 Ma. The postulated plume activity at c. 2800 Ma was the precursor for a protracted series of events that would eventually lead to cratonization of the domain (Fig. 9c).

A diverse although systematically evolving range of granitic compositions ensued from c. 2760 to c. 2600 Ma. During this period, the intrusion of primitive, isotopically juvenile hornblende tonalites progressively evolved to more fractionated compositions. Granites were also sourced at progressively shallower levels, which is likely the result of conductive heat transferring upwards after the final greenstone successions had been deposited (Fig. 9c). This evolution signifies not only nearly continuous crustal melting over this period, but a change in the source of melts, from early melting of deep-crustal amphibolites (generating TTG), to later melting of mid-crustal rocks (the older TTG, generating monzogranites of the Tuckanarra and Jungar Suites), and potential remelting of these and older basement material to generate the Bald Rock Supersuite.

This continuous and progressive evolution of melts finally resulted in cratonization of the domain, probably causing nearly complete depletion of the lower–mid crust. During the most vigorous granitic activity from c. 2700 to c. 2650 Ma this depletion likely resulted in the composition of the lower–mid crust changing from amphibolite to depleted, garnet-bearing granulite. Weakness in the lower–mid crust due to the extent of melting at this time may be responsible for greenstone sinking and soft-crust deformation (Fig. 9c). Significantly, the change in granite compositions at c. 2645 Ma is interpreted to reflect renewed heat input to the base of the crust, potentially as a result of delamination of garnet-rich,

lower crustal residuum such as an eclogitic layer (Fig. 9c; Smithies and Champion, 1999). This process would have allowed melts to source more evolved material as shown by more negative ϵ_{Hf} compositions at this time (Fig. 9a). Delamination is also one mechanism that could allow widespread melts (Bald Rock Supersuite) to continue for such an extended period and cause the final phase of cratonization of the domain.

A model for such a protracted succession of melting events would certainly become more feasible with a mechanism for significant upper crustal insulation. If effective over long periods, this could negate the necessity for a major delamination event. The greenstone blanketing effect (Rey et al., 2003) suggested for the period 2750–2650 Ma is compatible with our model (see ‘blanketing’ in Fig. 9c), where we suggest this effect to be most important from 2720 to 2680 Ma.

The process of intra-crustal differentiation, as proposed for EGST (Campbell and Hill, 1988; Hill et al., 1989) may be applicable in the Murchison Domain and is also consistent with a heat source of plume origin. The shallowing of depth of melting in the Murchison Domain granitic rocks from c. 2765–2600 Ma, as documented by the progressive evolution of the Sm–Nd isotope system (Champion and Cassidy, 2002) and also the Lu–Hf system (this study), indicates that this differentiation through time and space is the key process that determined the structure and composition of this part of the Yilgarn Craton, leading up to its cratonization and stabilization.

Relation to seismic data

Recent deep seismic and magnetotelluric surveys in the northern Yilgarn Craton reveal continuation of the Yarraquin Seismic Province from Narryer to the Youanmi Terrane (Geological Survey of Western Australia, 2013). This province occurs close to the surface in the Narryer Terrane and it apparently underlies the upper crustal rocks of the rest of the Murchison and Southern Cross domains of the Youanmi Terrane, typically at a depth of 10 km. Therefore a terrane accretion model for the formation of the northern Yilgarn Craton with the Narryer Terrane as a thrust exotic block (Nutman et al., 1993) appears inconsistent with this dataset.

In terms of Lu–Hf isotopic data presented in this study, Narryer Terrane-aged material is consistently sampled by granites across the area of study. This suggests the material within the Yarraquin Seismic Province is isotopically similar in both the Narryer and Youanmi Terranes. Differential uplift associated with Proterozoic unroofing of the Narryer Terrane is the simplest explanation for the seismic data. Differential uplift is consistent with an autochthonous development of the Narryer and Youanmi Terranes (cf. Van Kranendonk et al., in press).

Conclusions

1. Lu–Hf isotopic data from zircons are consistent with an autochthonous development for the Murchison Domain. We propose multiple mantle plumes at

2.81 and 2.72 Ga as the driving force for crustal development (i.e. melting and reworking) in the Murchison Domain from 2820 to 2600 Ma.

2. Lu–Hf isotopic data from zircons are consistent with seismic interpretations in that they both suggest sampling of older, Narryer Terrane-like crust within the Murchison Domain. This is interpreted to be evidence in favour of an autochthonous development of the Youanmi Terrane.
3. ϵ_{Hf} values in felsic rocks during deposition of the Norie, Polelle, and Glen Groups of the northern Murchison Domain indicate continued juvenile input into the crust over the period of their formation from 2820 to 2700 Ma.
4. Depleted mantle model ages reveal that zircons from the northern Murchison Domain continued tapping of a c. 3.0 Ga mantle source from 2820 to 2640 Ma. This indicates a significant crust-forming juvenile event at c. 3.0 Ga.
5. The c. 3.80 Ga source material sampled appears to be related to the complex early history of the Yilgarn Craton, possibly represented by the >3.0 Ga rocks in the Narryer Terrane, which may lie underneath the Murchison Domain.
6. The Polelle Group is unique in that it has sampled source material with model ages of both 3.04 Ga and 3.80 Ga, indicating this as the most significant crustal reworking event in the Murchison Domain at c. 2750 Ma. This event is also accompanied by melt sources that are diverse both in terms of geochemistry and depth. Mafic–felsic magma mixing may account for the range of geochemical and isotopic compositions at this time.
7. A period of blanketing and crustal overturn is proposed from c. 2720 to c. 2660 Ma and may be responsible for continued granitic magmatism of the Bald Rock Supersuite.
8. Granitic magmatism that post-dates the greenstones has Lu–Hf compositions consistent with both the mixing of juvenile and older crust and also recycling of the c. 3.04 Ga and the c. 3.80 Ga model aged sources. However, the Bald Rock Supersuite lacks the more juvenile component.
9. Secular geochemical trends indicate that, over an extended period from c. 2750 to 2600 Ma, granitic rocks became progressively more fractionated, involved more extensive crustal remelting, and were sourced at shallower levels.

Acknowledgements

The authors thank Hugh Smithies, David Champion, and Paul Morris for helpful discussions. Suzanne Dowsett and Michael Prause are thanked for drafting the figures. Staff at the ARC National Key Centre for Geochemical Evolution and Metallogeny of Continents (GEMOC) and Carlisle Labs are thanked for their sample handling.

References

- Barley, ME, Brown, SJA, Krapež, B and Kositsin, N 2008, Physical volcanology and geochemistry of a Late Archaean volcanic arc: Kurnalpi and Gindalbie Terranes, Eastern Goldfields Superterrane, Western Australia: *Precambrian Research*, v. 161, p. 53–76.
- Barley, ME, Kerrich, R, Reudavy, I and Xie, Q 2000, Late Archaean Ti-rich, Al-depleted komatiites and komatiitic volcanoclastic rocks from the Murchison Terrane in Western Australia: *Australian Journal of Earth Sciences*, v. 47, no. 5, p. 873–883.
- Blichert-Toft, J and Albarède, F 1997, The Lu–Hf isotope geochemistry of chondrites and the evolution of the mantle–crust system: *Earth and Planetary Science Letters*, v. 148, no. 1–2, p. 243–258, doi: 10.1016/S0012-821X(97)00040-X.
- Campbell, IH and Hill, RI 1988, A two-stage model for the formation of the granite–greenstone terrains of the Kalgoorlie–Norseman area, Western Australia: *Earth and Planetary Science Letters*, v. 90, p. 11–25.
- Campbell, IH and Griffiths, RW 1990, Implications of mantle plume structure for the evolution of flood basalts: *Earth and Planetary Science Letters*, v. 99, p. 79–93.
- Cassidy, KF, Champion, DC, Krapež, B, Barley, ME, Brown, SJA, Blewett, RS, Groenewald, PB and Tyler, IM 2006, A revised geological framework for the Yilgarn Craton, Western Australia: Geological Survey of Western Australia, Record 2006/8, 8p.
- Champion, DC and Cassidy, KF 2002, Granites of the northern Murchison Province: their distribution, age, geochemistry, petrogenesis, relationship with mineralisation, and implications for tectonic environment, in *The characterisation and metallogenic significance of Archaean granitoids of the Yilgarn Craton* edited by KF Cassidy, DC Champion, NJ McNaughton, IR Fletcher, AJ Whitaker, IV Bastrakova and A Budd: Minerals and Energy Research Institute of Western Australia (MERIWA), Project no. M281/AMIRA Project no. 482 (unpublished report no. 222), p. 1–54.
- Champion, DC and Cassidy, KF 2010, Granitic magmatism in the Yilgarn Craton: implications for crustal growth and metallogeny, in *Yilgarn Superior Workshop — Abstracts* edited by S Wyche: Geological Survey of Western Australia; Fifth International Archaean Symposium, Perth, Western Australia, Record 20, p. 12–18.
- Champion, DC and Sheraton, JW 1997, Geochemistry and Nd isotope systematics of Archaean granites of the Eastern Goldfields, Yilgarn Craton, Australia: implications for crustal growth processes: *Precambrian Research*, v. 83, p. 109–132.
- Czarnota, K, Champion, DC, Goscombe, B, Blewett, RS, Cassidy, KF, Henson, PA and Groenewald, PB 2010, Geodynamics of the eastern Yilgarn Craton: *Precambrian Research*, v. 183, p. 175–202.
- De Oliveira, MA, Dall’Agnol, R and Scaillet, B 2010, Petrological constraints on crystallization conditions of Mesoarchean sanukitoid rocks, southeastern Amazonian Craton, Brazil: *Journal of Petrology*, v. 51, no. 10, p. 2121–2148.
- DeBievre, P and Taylor, PDP 1993, Table of the isotopic composition of the elements: *International Journal of Mass Spectrometry and Ion Processes*, v. 123, p. 149.
- Eggins, SM, Woodhead, JD, Kinsley, LPJ, Mortimer, GE, Sylvester, PJ, McCulloch, MT, Hergt, JM and Handler, MR 1997, A simple method for the precise determination of >40 trace elements in geological samples by ICPMS using enriched isotope internal standardisation: *Chemical Geology*, v. 134, p. 311–326.
- Geological Survey of Western Australia 2013, Youanmi and Southern Carnarvon seismic and magnetotelluric (MT) workshop (preliminary edition): Geological Survey of Western Australia, Record 2013/6, 171p.
- Goolaerts, A, Mattioli, N, de Jong, J, Weis, D and Scoates, JS 2004, Hf and Lu isotopic reference values for the zircon standard 91500 by MC-ICP-MS: *Chemical Geology*, v. 206, p. 1–9.

- Griffin, WL, Belousova, EA, Shee, SR, Pearson, NJ and O'Reilly, SY 2004, Archean crustal evolution in the northern Yilgarn Craton: U–Pb and Hf-isotope evidence from detrital zircons: *Precambrian Research*, v. 127, p. 19–41.
- Griffin, WL, Pearson, NJ, Belousova, EA, Jackson, SE, O'Reilly, SY, van Achterbergh, E and Shee, SR 2000, The Hf isotope composition of cratonic mantle: LAM-MC-ICPMS analysis of zircon megacrysts in kimberlites: *Geochimica et Cosmochimica Acta*, v. 64, p. 133–147.
- Griffin, WL, Pearson, NJ, Belousova, EA and Saeed, A 2006, Comment: Hf-isotope heterogeneity in standard zircon 91500: *Chemical Geology*, v. 233, p. 358–363.
- Griffin, WL, Pearson, NJ, Belousova, EA and Saeed, A 2007, Reply to 'Comment to short-communication 'Comment: Hf-isotope heterogeneity in zircon 91500' by WL Griffin, NJ Pearson, EA Belousova, A, Saeed (Chemical Geology 233 (2006) p. 358–363)' by F Corfu: *Chemical Geology*, v. 244, p. 354–356.
- Griffin, WL, Wang, X, Jackson, SE, Pearson, NJ, O'Reilly, SY, Xu, X and Zhou, X 2002, Zircon chemistry and magma genesis, SE China: in-situ analysis of Hf isotopes, Pingtan and Tonglu igneous complexes: *Lithos*, v. 61, p. 237–269.
- Hill, RE, Campbell, IH and Compston, W 1989, Age and origin of granitic rocks of the Kalgoorlie–Norseman region, Western Australia: implications for the origin of Archean crust: *Geochimica et Cosmochimica Acta*, v. 53, p. 1259–1275.
- Ivanic, TJ, Van Kranendonk, MJ, Kirkland, CL, Wyche, S, Wingate, MTD and Belousova, E 2012, Zircon Lu–Hf isotopes and granite geochemistry of the Murchison Domain of the Yilgarn Craton: evidence for reworking of Eoarchean crust during Meso–Neoarchean plume-driven magmatism: *Lithos*, v. 148, p. 112–127.
- Ivanic, TJ, Wingate, MTD, Kirkland, CL, Van Kranendonk, MJ and Wyche, S 2010, Age and significance of voluminous mafic–ultramafic magmatic events in the Murchison Domain, Yilgarn Craton: *Australian Journal of Earth Sciences*, v. 57, p. 597–614.
- Kinny, PD, Williams, IS, Froude, DO, Ireland, TR and Compston, W 1988, Early Archean zircon ages from orthogneisses and anorthosites at Mount Narryer, Western Australia: *Precambrian Research*, v. 38, p. 325–341.
- Kositcin, N, Brown, SJA, Barley, ME, Krapež, B, Cassidy, KF and Champion, DC 2008, SHRIMP U–Pb zircon age constraints on the Late Archean tectonostratigraphic architecture of the Eastern Goldfields Superterrane, Yilgarn Craton, Western Australia: *Precambrian Research*, v. 161, p. 5–33.
- Martin, H, Smithies, RH, Rapp, R, Moyen, J-F and Champion, DC 2005, An overview of adakite, tonalite–trondhjemite–granodiorite (TTG), and sanukitoid: relationships and some implications for crustal evolution: *Lithos*, v. 79, p. 1–24.
- Morris, PA and Witt, WK 1997, Geochemistry and tectonic setting of two contrasting Archean felsic volcanic associations in the Eastern Goldfields, Western Australia: *Precambrian Research*, v. 83, p. 83–107.
- Moyen, J-F, Champion, DC and Smithies, RH 2009, The geochemistry of Archean plagioclase-rich granites as a marker of source enrichment and depth of melting: *Earth and Environmental Science Transactions of the Royal Society of Edinburgh*, v. 100, p. 35–50.
- Murakami, T, Chakoumakos, BC, Ewing, RC, Lumpkin, GR and Weber, WJ 1991, Alpha-decay event damage in zircon: *American Mineralogist*, v. 76, p. 1510–1532.
- Myers, JS 1988, Early Archean Narryer Gneiss Complex, Yilgarn Craton, Western Australia: *Precambrian Research*, v. 38, p. 279–307.
- Myers, JS 1995, The generation and assembly of an Archean supercontinent: evidence from the Yilgarn Craton, Western Australia, in *Early Precambrian Processes* edited by MP Coward and AC Reis: Geological Society, London, Special Publication 95, p. 143–154.
- Nelson, DR 2001, 169003: vesicular rhyolite, Carron Hill: *Geochronology Record* 170: Geological Survey of Western Australia, 4p.
- Nelson, DR, Robinson, BW and Myers, JS 2000, Complex geological histories extending for >4.0 Ga deciphered from xenocryst zircon microstructures: *Earth and Planetary Science Letters*, v. 181, p. 89–102.
- Norrish, K and Chappell, BW 1977, X-ray fluorescence spectrometry, in *Physical methods in determinative mineralogy* (2nd edition) edited by J Zussman: Academic Press, London, UK, p. 201–272.
- Norrish, K and Hutton, JT 1969, An accurate X-ray spectrographic method for the analysis of a wide range of geological samples: *Geochimica et Cosmochimica Acta*, v. 33, no. 4, p. 431–453.
- Nowell, GM, Kempton, PD, Noble, SR, Fitton, JG, Saunders, AD, Mahoney, JJ and Taylor, RN 1998, High precision Hf isotope measurements of MORB and OIB by thermal ionisation mass spectrometry: insights into the depleted mantle: *Chemical Geology*, v. 149, p. 211–233.
- Nutman, AP, Bennett, VC, Kinny, PD and Price, R 1993, Large-scale crustal structure of the northwestern Yilgarn Craton, Western Australia: evidence from Nd isotopic data and zircon geochronology: *Tectonics*, v. 12, p. 971–981.
- Pearce, JA 2008, Geochemical fingerprinting of oceanic basalts with applications to ophiolite classification and the search for Archean oceanic crust: *Lithos*, v. 100, p. 14–48.
- Pyke, J 2000, Minerals laboratory staff develops ICP-MS preparation method: *Australian Geological Survey Organisation Newsletter*, v. 33, p. 12–14.
- Rey, PF, Philippot, P and Thébaud, N 2003, Contribution of mantle plumes, crustal thickening and greenstone blanketing to the 2.75–2.65 Ga global crisis: *Precambrian Research*, v. 127, p. 43–60.
- Schaltegger, U and Krähenbühl, U 1990, Heavy rare-earth element enrichment in granites of the Aar Massif (Central Alps, Switzerland): *Chemical Geology*, v. 89, p. 49–63.
- Scherer, E, Münker, C and Mezger, K 2001, Calibration of the lutetium–hafnium clock: *Science*, v. 293, p. 683–687.
- Smithies, RH and Champion, DC 1999, High-Mg diorite from the Archean Pilbara Craton; anorogenic magmas derived from a subduction-modified mantle, in *Geological Survey of Western Australia Annual Review 1998–99*: Geological Survey of Western Australia, Perth, Western Australia, p. 45–50.
- Sun, S-S and McDonough, WF 1989, Chemical and isotopic systematics of oceanic basalts: implications for mantle compositions and processes, in *Magmatism in the Ocean Basins* edited by AD Saunders and MJ Norry: Geological Society, London, Special Publication 42, p. 313–345.
- Taylor, SR and Hallberg, JA 1977, Rare-earth elements in the Marda calc-alkaline suite: an Archean geochemical analogue of Andean-type volcanism: *Geochimica et Cosmochimica Acta*, v. 41, no. 8, p. 1125–1129.
- Van Kranendonk, MJ and Ivanic, TJ 2009, A new lithostratigraphic scheme for the northeastern Murchison Domain, Yilgarn Craton, in *Geological Survey of Western Australia Annual Review 2007–08*: Geological Survey of Western Australia, Perth, Western Australia, p. 34–53.
- Van Kranendonk, MJ, Ivanic, TJ, Wingate, MTD, Kirkland, L and Wyche, S 2013, Long-lived, autochthonous development of the Archean Murchison Domain, Yilgarn Craton: *Precambrian Research*.
- Van Kranendonk, MJ, Ivanic, TJ, Wyche, S, Wilde, SA and Zibra, I (compilers) 2010, A time transect through the Hadean to Neoproterozoic geology of the western Yilgarn Craton — a field guide: Geological Survey of Western Australia, Record 2010/19, 69p.

- Wang, Q 1998, Geochronology of the granite–greenstone terranes in the Murchison and Southern Cross Provinces of the Yilgarn Craton, Western Australia: Australian National University, Canberra, PhD thesis (unpublished), 186p.
- Wang, Q, Schiøtte, L and Campbell, IH 1998, Geochronology of supracrustal rocks from the Golden Grove area, Murchison Province, Yilgarn Craton, Western Australia: Australian Journal of Earth Sciences, v. 45, p. 571–577.
- Watkins, KP and Hickman, AH 1990, Geological evolution and mineralization of the Murchison Province, Western Australia: Geological Survey of Western Australia, Bulletin 137, 267p.
- Wilde, SA, Middleton, MF and Evans, BJ 1996, Terrane accretion in the southwestern Yilgarn Craton: evidence from a deep seismic crustal profile: Precambrian Research, v. 78, p. 179–196.
- Willbold, M, Hegner, E, Stracke, A and Rocholl, A 2009, Continental geochemical signatures in dacites from Iceland and implications for models of early Archaean crust formation: Earth and Planetary Science Letters, v. 279, p. 44–52.
- Wingate, MTD, Bodorkos, S and Forbes, CJ 2009a, 178141: quartz diorite, Callisto Mine; Geochronology Record 786: Geological Survey of Western Australia, 4p.
- Wingate, MTD, Bodorkos, S and Kirkland, CL 2008a, 178102: hornblende tonalite, Finger Post Bore; Geochronology Record 727: Geological Survey of Western Australia, 4p.
- Wingate, MTD, Bodorkos, S and Kirkland, CL 2008b, 178103: biotite monzogranite, Cement Tank Well; Geochronology Record 728: Geological Survey of Western Australia, 4p.
- Wingate, MTD, Bodorkos, S and Kirkland, CL 2008c, 178105: andesite, Woolgra Bore; Geochronology Record 730: Geological Survey of Western Australia, 4p.
- Wingate, MTD, Bodorkos, S and Van Kranendonk, MJ 2009b, 178197: biotite monzogranite, Milliewarrie Well; Geochronology Record 790: Geological Survey of Western Australia, 4p.
- Wingate, MTD, Bodorkos, S and Van Kranendonk, MJ 2009c, 178199: foliated granodiorite, Jungar Pool; Geochronology Record 791: Geological Survey of Western Australia, 4p.
- Wingate, MTD, Kirkland, CL and Chen, SF 2012a, 185932: metarhyolite, Eelya Hill; Geochronology Record 1007: Geological Survey of Western Australia, 4p.
- Wingate, MTD, Kirkland, CL and Forbes, CJ 2011a, 178142: metarhyolite, Cullculli Hill; Geochronology Record 967: Geological Survey of Western Australia, 4p.
- Wingate, MTD, Kirkland, CL and Ivanic, TJ 2010a, 185927: leucogabbro sill, Barloweerinyer Hill; Geochronology Record 892: Geological Survey of Western Australia, 4p.
- Wingate, MTD, Kirkland, CL and Ivanic, TJ 2011b, 185929: granodiorite, Wogala Bore; Geochronology Record 972: Geological Survey of Western Australia, 4p.
- Wingate, MTD, Kirkland, CL and Ivanic, TJ 2012b, 193972: metarhyolite clast in volcanoclastic breccia, Weld Range; Geochronology Record 1011: Geological Survey of Western Australia, 4p.
- Wingate, MTD, Kirkland, CL and Van Kranendonk, MJ 2010b, 185922: leucogabbro sill, Fleece Pool; Geochronology Record 891: Geological Survey of Western Australia, 4p.
- Wingate, MTD, Kirkland, CL and Van Kranendonk, MJ 2010c, 185933: biotite granodiorite, Eelya North Mine; Geochronology Record 894: Geological Survey of Western Australia, 4p.
- Wingate, MTD, Kirkland, CL and Van Kranendonk, MJ 2011c, 178196: granodiorite, Milliwarry Well; Geochronology Record 968: Geological Survey of Western Australia, 4p.
- Wingate, MTD, Kirkland, CL and Van Kranendonk, MJ 2011d, 185923: biotite–hornblende tonalite gneiss, Granite Rock; Geochronology Record 970: Geological Survey of Western Australia, 4p.
- Wingate, MTD and Van Kranendonk, MJ 2009, 178194: granite orthogneiss, Coodardy Homestead; Geochronology Record 788: Geological Survey of Western Australia, 4p.
- Wyche, S 2007, Evidence of pre-3100 Ma crust in the Youanmi and Southwest Terranes and Eastern Goldfields Superterrane, of the Yilgarn Craton, in *Earth's Oldest Rocks edited by MJ Van Kranendonk, RH Smithies and VC Bennett: Elsevier BV, Developments in Precambrian Geology 15*, p. 113–123.
- Wyche, S, Kirkland, CL, Riganti, A, Pawley, MJ, Belousova, E and Wingate, MTD 2012, Isotopic constraints on stratigraphy in the central and eastern Yilgarn Craton, Western Australia: Australian Journal of Earth Sciences, v. 59, no. 5 (Archean evolution — Yilgarn Craton), p. 657–670, doi:10.1080/08120099.2012.697677.
- Yeats, CJ, McNaughton, NJ and Groves, DI 1996, SHRIMP U–Pb geochronological constraints on Archean volcanic-hosted massive sulfide and lode gold mineralization at Mount Gibson, Yilgarn Craton, Western Australia: Economic Geology, v. 91, p. 1354–1371.
- Zibra, I 2012, Syndeformational granite crystallisation along the Mount Magnet Greenstone Belt, Yilgarn Craton: evidence of large-scale magma-driven strain localisation during Neoproterozoic time: Australian Journal of Earth Sciences, v. 59, no. 5, p. 793–806.

Appendix

Analytical results and geochemical model

Table A1.1. Major and trace element geochemistry for northern Murchison Domain samples

Granitic Suite	GSWA number	Latitude	Longitude	Easting	Northing	Lithname	Site ID	SiO ₂ (%)	TiO ₂ (%)	Al ₂ O ₃ (%)	Fe ₂ O ₃ ^t (%)	FeO (%)	MnO (%)	MgO (%)	CaO (%)	Na ₂ O (%)	K ₂ O (%)	P ₂ O ₅ (%)	SO ₃ (%)	LOI (%)	Cs (ppm)	Rb (ppm)	Ba (ppm)	Th (ppm)	Ta (ppm)
Mount Kenneth Suite	191037	-27.9169	118.3950	637272	6911218	pegmatite	TJWIN000261	75.83	0.06	13.60	0.76	0.09	0.01	0.24	0.65	4.25	3.79	0.02	0.08	0.65	2.9	134.0	988.0	11.3	0.8
Mount Kenneth Suite	193987	-27.9732	118.4864	646191	6904872	granodiorite	TJWIN090455	74.22	0.55	11.11	2.70	1.63	0.02	5.26	0.10	0.17	1.75	0.08	0.01	3.95	0.1	36.8	133.0	16.1	2.9
Annean Supersuite	178104	-26.7942	118.2926	628483	7035709	granitic rock	CJFMEE000474													1.5	93.5	672.2	13.0	0.8	
Annean Supersuite	178104	-26.7942	118.2926	628483	7035709	granitic rock	CJFMEE000474	76.72	0.10	12.46	1.32	0.07	0.02	0.16	1.00	4.55	2.51	0.03	0.01	1.01	n.d.	83.3	583.0	14.0	
Annean Supersuite	178193	-27.0710	118.4210	640902	7004908	granitic rock	MTWREE000067	70.15	0.23	15.62	1.64		0.03	0.38	1.45	5.12	4.17	0.06		0.28	1.5	110.0	3280.0	17.4	n.d.
Annean Supersuite	178193	-27.0710	118.4210	640902	7004908	granitic rock	MTWREE000067	70.76	0.22	15.75	1.69	0.55	0.03	0.38	1.46	5.23	4.20	0.06	0.02	n.d	1.6	113.5	3499.0	17.6	0.2
Annean Supersuite	178194	-27.2333	117.6669	566032	6987547	metagranitic rock	MTWCUE000068	71.91	0.14	14.96	1.20		0.03	0.20	0.87	4.02	5.74	0.04		0.31	3.9	260.0	2460.0	22.1	0.2
Annean Supersuite	178194	-27.2333	117.6669	566032	6987547	metagranitic rock	MTWCUE000068	71.29	0.13	14.77	1.17	0.26	0.03	0.19	0.87	4.01	5.71	0.04	0.02	1.40	4.5	261.5	2694.0	22.6	0.7
Annean Supersuite	178196	-27.1197	117.5900	558474	7000166	granodiorite	MTWCUE000069	68.33	0.34	14.94	3.23		0.04	1.65	2.69	4.57	2.96	0.13		0.68	11.7	122.0	2370.0	13.2	-0.1
Annean Supersuite	178196	-27.1197	117.5900	558474	7000166	granodiorite	MTWCUE000069	68.01	0.33	14.85	3.25	1.20	0.04	1.63	2.71	4.61	2.97	0.13	0.01	1.03	14.4	123.6	2547.0	11.2	0.2
Annean Supersuite	178198	-27.0904	117.7275	572118	7003343	monzogranite	MTWCUE000071	70.86	0.21	14.98	1.77		0.04	0.50	1.13	4.29	5.26	0.07		0.37	3.8	262.0	2570.0	29.5	0.5
Annean Supersuite	178198	-27.0904	117.7275	572118	7003343	monzogranite	MTWCUE000071	70.66	0.20	14.89	1.77	0.40	0.04	0.49	1.14	4.30	5.24	0.07	0.01	0.79	4.0	247.4	2576.0	27.2	0.9
Annean Supersuite	185920	-27.0749	117.7311	572484	7005055	granitic rock	MTWCUE000092	71.85	0.10	14.36	1.03	0.07	0.03	0.14	0.72	4.14	5.67	0.03	0.01	1.59	5.4	316.2	2157.0	21.7	0.9
Annean Supersuite	185921	-27.1535	117.5950	558948	6996425	monzogranite	MTWCUE000093	70.22	0.27	15.17	2.07	0.72	0.03	0.49	1.63	4.84	3.39	0.12	0.02	1.40	2.0	91.9	2201.0	8.8	0.2
Annean Supersuite	187665	-26.0149	118.1715	617235	7122142	monzogranite	SFCMTI001036														0.2	186.2	1074.0	45.0	0.1
Annean Supersuite	187665	-26.0149	118.1715	617235	7122142	monzogranite	SFCMTI001036	74.11	0.17	13.54	1.36	0.43	0.02	0.25	1.07	3.53	5.18	0.05	0.01	0.56	n.d.	158.7	892.0	42.0	
Annean Supersuite	190525	-27.2109	117.9598	595052	6989845	metagranitic rock	MVKCUE070145														1.6	39.2	429.6	4.4	0.2
Annean Supersuite	190525	-27.2109	117.9598	595052	6989845	metagranitic rock	MVKCUE070145	71.02	0.30	15.19	1.90	0.86	0.02	0.72	2.56	6.02	0.76	0.13	0.04	1.20	n.d.	37.9	394.0	3.0	
Annean Supersuite	190907	-26.8390	177.8858	588009	7031088	felsic intrusive porphyry	TJIMDG000297	70.18	0.42	15.34	2.69	0.86	0.04	0.82	2.57	4.94	2.59	0.17	0.04		1.4	69.4	1168.0	7.1	0.3
Annean Supersuite	190935	-26.6986	117.9854	598032	7046564	granitic rock	TJIMDG000481	77.86	0.18	12.13	0.61	0.04	n.d.	0.06	0.33	3.91	4.67	0.06	0.05	0.04	4.0	281.9	212.0	34.2	1.4
Culculli Suite	190934	-26.6986	117.9854	598032	7046564	tonalite	TJIMDG000481	67.24	0.54	13.89	4.22	1.67	0.06	2.10	3.21	3.92	3.22	0.23	0.08	1.06	1.4	101.7	1184.0	19.1	0.4
Culculli Suite	190541	-27.3603	117.6142	560738	6973509	metatonalite	MVKCUE070251	66.47	0.34	15.24	2.75	0.94	0.05	0.74	1.52	4.85	5.61	0.13	0.02	1.88	0.8	275.3	2301.0	74.1	0.9
Culculli Suite	81760	-27.3888	117.8769	586700	6970200	metatonalite	GSD081760	66.10	0.42	15.30	4.58	2.50	0.04	1.56	3.82	4.39	1.58	0.11		1.23	1.7	62.0	562.0	11.2	1.1
Culculli Suite	185928	-26.7219	117.9720	596673	7044003	tonalite	MTWMAD000100	64.50	0.49	14.49	4.65	2.26	0.10	2.20	3.27	3.88	3.36	0.21	0.03	2.58	15.3	303.0	1083.0	19.1	0.7
Culculli Suite	178141	-27.0921	118.2986	628751	7002698	quartz diorite	MTWREE000080	62.03	0.55	14.39	5.56	3.40	0.07	4.41	5.00	3.88	1.45	0.16	0.01	2.34	1.8	38.0	563.2	7.9	0.3
Culculli Suite	185923	-27.4119	117.6962	568818	6967748	dioritic gneiss	MTWCUE000095	65.63	0.46	16.92	4.24	2.72	0.06	2.10	4.56	4.15	1.59	0.15	0.02	0.01	9.0	154.2	255.0	4.5	1.6
Eelya Suite	185933	-27.3489	118.1628	615014	6974387	granitic rock	MTWREE000105	75.38	0.23	12.14	2.01	1.39	0.03	0.31	1.50	4.13	2.26	0.04	0.59	1.26	6.9	65.5	761.1	13.1	0.7
Big Bell Suite	178192	-27.1550	118.3241	631198	6995703	monzogranite	MTWREE000066	71.94	0.28	14.91	1.79		0.03	0.52	1.77	4.87	3.04	0.10		0.48	0.8	86.0	1580.0	17.2	0.1
Big Bell Suite	178192	-27.1550	118.3241	631198	6995703	monzogranite	MTWREE000066	71.38	0.28	14.68	1.82	0.57	0.02	0.50	1.76	4.84	3.02	0.10	0.01	1.33	0.9	78.3	1679.0	15.4	0.3
Tuckanarra Suite	178190	-27.0653	118.1406	613102	7005825	monzogranite	MTWREE000064	73.35	0.23	14.40	1.63		0.03	0.38	1.51	4.53	3.13	0.07		0.41	2.8	117.0	778.0	17.3	0.2
Tuckanarra Suite	178190	-27.0653	118.1406	613102	7005825	monzogranite	MTWREE000064	72.73	0.22	14.28	1.58	0.44	0.03	0.36	1.51	4.53	3.11	0.07	0.01	1.43	3.1	120.0	799.6	17.0	0.7
Tuckanarra Suite	178199	-27.0238	117.9408	593322	7010580	granodiorite	MTWCUE000072	74.25	0.20	13.54	1.61	0.20	0.04	0.32	1.37	3.64	4.55	0.07	0.01	0.29	2.5	227.9	552.4	30.9	1.5
Tuckanarra Suite	178199	-27.0238	117.9408	593322	7010580	granodiorite	MTWCUE000072	73.98	0.20	13.52	1.59		0.04	0.32	1.35	3.60	4.50	0.07		0.42	2.2	218.0	554.0	28.9	0.6
Tuckanarra Suite	180087	-27.0228	117.9414	593386	7010694	metamonzogranite	MVKCUE060128	72.29	0.25	13.49	1.81	1.37	0.05	0.41	1.48	3.71	4.23	0.09	n.d.	2.08	6.4	243.4	506.2	32.4	1.9
Tuckanarra Suite	184111	-27.1366	118.2815	626994	6997789	felsic porphyry dyke	SXWMEE000023	75.24	0.07	13.95	0.85	0.37	0.03	0.15	0.94	7.03	0.63	0.05	0.03	0.97	1.5	19.2	331.3	9.3	
Jungar Suite	81770	-27.4959	117.9223	591100	6958300	granodiorite	GSD081770	69.20	0.36	14.70	3.18	1.42	0.02	1.12	2.61	4.37	2.04	0.14		0.91	2.4	81.0	596.0	12.2	1.1
Jungar Suite	178101	-26.6487	118.4128	640612	7051696	granitic rock	CJFMEE000222														4.1	157.2	1249.0	27.6	1.0
Jungar Suite	178101	-26.6487	118.4128	640612	7051696	granitic rock	CJFMEE000222	72.88	0.26	14.28	1.77	0.68	0.03	0.41	1.66	4.05	3.92	0.07	0.01	0.48	n.d.	136.8	1100.0	30.0	
Jungar Suite	178102	-26.7452	118.3039	629667	7041124	granitic rock	CJFMEE000263	63.84	0.56	14.69	5.72	3.28	0.08	2.69	4.97	3.78	1.18	0.15	0.01	2.20	4.9	53.6	379.4	8.0	0.5
Jungar Suite	178103	-26.7347	118.2649	625801	7042319	granitic rock	CJFMEE000267														6.4	222.9	1374.0	33.8	1.5
Jungar Suite	178103	-26.7347	118.2649	625801	7042319	granitic rock	CJFMEE000267	71.30	0.50	14.20	2.58	1.29	0.03	0.49	1.65	4.03	4.27	0.14	0.01	0.54	n.d.	195.4	1252.0	41.0	
Jungar Suite	187640	-26.3572	118.2779	627502	7084129	monzogranite	SFCMTI000806														2.9	104.8	558.5	9.5	0.8
Jungar Suite	187640	-26.3572	118.2779	627502	7084129	monzogranite	SFCMTI000806	71.31	0.31	15.06	1.96	0.95	0.03	0.69	2.36	5.00	2.08	0.12	0.02	0.96	n.d.	84.9	443.0	8.0	
Jungar Suite	187649	-26.3256	118.2618	625934	7087646	monzogranite	SFCMTI000869														6.2	246.9	974.3	37.4	4.5
Jungar Suite	187649	-26.3256	118.2618	625934	7087646	monzogranite	SFCMTI000869	74.11	0.12	13.83	1.27	0.47	0.04	0.21	1.14	3.73	4.75	0.05	0.01	0.58	6.0	218.7	830.0	34.0	
Jungar Suite	187651	-26.2281	118.2427	624135	7098456	monzogranite	SFCMTI000909														1.5	181.7	1714.0	82.2	0.3
Jungar Suite	187651	-26.2281	118.2427	624135	7098456	monzogranite	SFCMTI000909	71.16	0.27	14.12	2.19	0.87	0.03	0.37	1.34	3.52	5.22	0.08	0.02	1.47	n.d.	148.6	1369.0	94.0	
Jungar Suite	187655	-26.2380	118.4616	645990	7097141	monzogranite	SFCMTI000972														9.5	314.5	868.7	65.0	2.1
Jungar Suite	187655	-26.2380	118.4616	645990	7097141	monzogranite	SFCMTI000972	73.33	0.16	13.78	1.52	0.72	0.04	0.27	1.16	3.43	5.31	0.05	0.01	0.80	8.0				

Table A1.1. continued

GSWA number	Nb (ppm)	La (ppm)	Ce (ppm)	Pr (ppm)	Sr (ppm)	Nd (ppm)	Zr (ppm)	Sm (ppm)	Eu (ppm)	Gd (ppm)	Tb (ppm)	Dy (ppm)	Y (ppm)	Ho (ppm)	Er (ppm)	Tm (ppm)	Yb (ppm)	Lu (ppm)	Cr (ppm)	Cu (ppm)	F (ppm)	Ga (ppm)	Ni (ppm)	Pb (ppm)	Sc (ppm)	V (ppm)	Zn (ppm)	Eu*	Nb*
191037	13.0	11.3	21.0	2.7	93.0	9.7	106.0	2.2	0.4	2.0	0.4	2.4	13.1	0.5	1.5	0.3	1.8	0.3	2.0	11.0	3066.0	178	30.0	25.0	2.0	15.0	8.0	0.58	0.24
193987	51.1	75.7	181.1	24.7	5.5	110.5	566.2	29.6	6.8	33.5	5.9	37.9	229.1	8.1	23.5		23.3	3.3	6.0	1.0	1174.0	15.8	3.0	6.0	16.9	5.0	9.0	0.66	0.48
178104	8.4	30.1	48.0	4.9	92.8	16.4	105.0	2.9	0.5	2.5	0.4	2.2	16.1	0.5	1.4		1.4	0.2	31.1	3.9		16.2	n.d.	16.3	4.5	2.8	25.4	0.51	0.12
178104	7.0	23.0	41.0		81.0	12.0	87.0						17.0						13.0	3.0	n.d.	14.2	3.0	13.0	2.0	3.0	23.0		0.10
178193	3.0	48.2	91.4	10.6	1290.0	39.4		6.3	1.7	4.0	0.5	2.0	8.9	0.3	0.8	0.1	0.7	0.1		2.0		19.8	10.0	51.0	2.0	15.0	44.0	0.94	0.03
178193	4.8	51.5	88.5	9.7	1331.1	36.0	220.0	6.0	1.6	4.0	0.6	2.1	13.0	0.5	0.7		1.1	0.1	2.0	1.0	941.0	20.3	4.0	50.5	3.5	12.0	50.0	0.94	0.05
178194	5.5	36.9	74.9	8.6	647.0	30.7		5.2	1.3	3.6	0.4	1.8	9.5	0.3	0.8	0.1	0.8	0.1		2.0		16.6	10.0	65.0	2.0	10.0	28.0	0.84	0.05
178194	8.9	40.7	75.5	8.3	657.5	30.0	154.0	5.5	1.4	3.8	0.6	2.3	14.0	0.5	0.8		1.2	0.2	3.0	-1.0	373.0	18.5	3.0	72.9	4.0	5.0	23.0	0.85	0.08
178196	2.5	58.2	114.0	12.5	964.0	43.3		5.9	1.5	3.0	0.3	1.3	6.1	0.2	0.5	0.1	0.5	0.1		2.0		18.8	50.0	18.0	5.0	40.0	38.0	0.97	0.03
178196	3.5	61.5	108.6	11.6	963.2	41.4	180.0	5.7	1.4	3.3	0.5	1.5	9.0	0.4	0.5		0.9	0.1	89.0	2.0	1729.0	20.1	42.0	18.1	5.7	41.0	33.0	0.92	0.04
178198	7.5	42.1	92.2	9.5	727.0	35.9		6.0	1.4	4.0	0.5	2.1	12.4	0.4	1.0	0.2	1.1	0.2		7.0		17.6	28.0	77.0	4.0	20.0	38.0	0.83	0.05
178198	10.7	42.1	84.3	8.7	708.9	32.0	185.0	5.7	1.4	3.9	0.6	2.4	16.0	0.5	1.0		1.3	0.2	15.0	6.0	801.0	17.7	12.0	73.7	5.3	15.0	40.0	0.83	0.08
185920	11.1	35.8	59.6	7.0	521.5	27.0	133.0	4.8	1.1	3.2	0.4	1.8	17.0	0.3	0.9		0.8	0.1	2.0	5.0	499.0	18.8	2.0	78.0	2.0	4.0	33.0	0.82	0.10
185921	3.3	43.2	75.1	8.5	793.2	29.4	170.0	4.2	1.0	2.2	0.2	0.9	7.0	0.1	0.3		0.2	n.d.	1.0	68.0	898.0	20.2	4.0	22.9	3.1	19.0	20.0	0.86	0.06
187665	7.9	55.7	117.2	12.2	112.5	39.8	175.3	7.7	0.6	6.2	0.8	4.6	21.2	0.8	1.9		1.1	0.2		n.d.		19.9		46.9	3.8			0.28	0.04
187665	6.0	50.0	95.0		98.6	32.0	137.0						21.0						n.d.	1.0		18.5	6.0	41.0	3.0	7.0	26.0		0.03
190525	2.9	15.4	28.4	2.7	386.3	10.2	119.7	1.6	0.5	1.2	0.1	0.6	3.5	0.1	0.3		0.2	0.0				21.1		9.3	3.5			1.04	0.11
190525	2.0	11.0	22.0		377.3	7.0	120.0						4.0						8.0	13.0	180.0	18.0	10.0	7.0	4.0	19.0	38.0		0.11
190907	4.0	38.5	55.9	6.9	583.9	24.8	130.0	3.8	1.5	2.6	0.3	0.6	9.1	0.3	1.0		0.5	0.1	4.0	2.0	418.0	18.8	19.7	18.0	3.5	34.0	34.0	1.38	0.08
190935	11.5	17.4	33.7	3.4	24.4	9.9	99.0	1.5	0.2	1.1	0.2	1.2	15.0	0.3	0.9		1.1	0.2	1.0	8.0	n.d.	13.5	8.0	19.0	2.3	6.0	10.0	0.38	0.08
190934	6.3	46.6	82.7	8.9	370.5	29.9	156.3	4.4	1.0	3.1	0.4	2.0	14.0	0.4	1.1		1.0	0.2	61.0	16.0	694.0	15.1	48.0	27.0	8.8	60.0	48.0	0.78	0.06
190541	15.8	62.1	108.5	11.3	852.9	38.0	364.0	6.4	1.5	4.2	0.5	2.5	19.0	0.4	1.1		1.1	0.2	12.0	6.0	1677.0	18.7	12.0	71.0	7.7	38.0	41.0	0.85	0.05
81760	11.0	26.4	50.5		168.0	18.0	148.0	3.6	0.9		0.7		27.0				2.5	0.4	24.0	24.0	360.0		61.0	10.0	9.9	63.0	42.0		
185928	8.6	48.1	86.2	8.9	391.7	32.9	161.0	5.3	1.2	3.6	0.5	2.5	19.0	0.5	1.3		1.4	0.2	67.0	89.0	8128.0	21.8	46.0	29.2	8.4	66.0	89.0	0.77	0.08
178141	5.8	25.3	45.5	5.1	295.5	18.9	137.0	3.6	1.1	3.5	0.6	3.0	18.0	0.7	1.7	0.3	1.8	0.3	220.0	4.0	408.0	17.0	135.0	6.0	14.8	97.0	42.0	0.91	0.12
185923	10.2	12.3	22.2	2.5	272.4	9.4	94.3	2.1	0.7	2.7	0.5	3.1	24.0	0.6	1.8		2.1	0.3	10.0	44.0	1194.0	22.9	26.0	13.0	11.1	95.0	53.0	0.90	0.41
185933	9.1	29.6	54.7	6.0	64.6	23.8	199.1	5.4	0.7	5.6	1.0	6.4	48.4	1.5	4.5		4.9	0.8	1.0	16.0	388.0	12.9	3.0	8.3	5.7	8.0	15.0	0.39	0.13
178192	4.5	52.7	100.0	10.4	653.0	37.7		5.2	1.3	3.0	0.4	1.7	8.7	0.3	0.8	0.1	0.8	0.1		4.0		19.8	20.0	30.0	3.0	20.0	44.0	0.89	0.05
178192	5.0	54.0	94.3	9.8	650.5	34.4	183.0	5.0	1.2	3.2	0.6	1.9	11.0	0.5	0.8		1.1	0.2	2.0	2.0	813.0	19.8	5.0	29.8	4.4	17.0	42.0	0.90	0.05
178190	4.0	33.9	63.7	6.6	303.0	24.6		3.9	0.9	3.0	0.4	1.8	9.4	0.3	0.9	0.1	0.8	0.1		10.0		20.6	20.0	33.0	3.0	15.0	52.0	0.78	0.04
178190	6.7	36.5	62.8	6.6	299.8	22.9	154.0	3.8	1.0	3.1	0.6	2.0	13.0	0.5	0.9		1.3	0.2	n.d.	5.0	458.0	20.8	5.0	33.0	4.3	14.0	43.0	0.87	0.07
178199	11.6	32.1	60.5	6.5	149.1	23.0	135.0	4.6	0.9	4.1	0.8	4.2	28.0	0.8	2.2		2.2	0.3	2.0	4.0	498.0	18.3	5.0	63.2	5.0	11.0	45.0	0.60	0.08
178199	5.5	30.8	65.9	6.9	143.0	25.3		4.8	0.7	4.4	0.7	4.0	23.3	0.9	2.7	0.4	2.4	0.3		4.0		18.6	20.0	60.0	3.0	10.0	46.0	0.46	0.04
180087	16.3	36.4	70.1	7.0	152.5	25.2	122.0	5.0	0.7	4.5	0.7	4.6	29.0	0.9	2.5		2.2	0.3	4.0	5.0	884.0	20.3	4.0	56.0	4.8	12.0	56.0	0.43	0.11
184111	6.2	22.1	44.0	4.8	154.8	16.5	68.5	2.6	0.5	2.0	0.3	1.4	7.2	0.2	0.6		0.6	0.1	24.0	4.0	n.d.	17.6	5.0	14.1	3.7	2.0	36.0	0.69	0.12
81770	8.0	36.3	70.2		428.0	27.5	121.0	4.2	1.1		0.4		8.0				0.6	0.1	20.0	25.0	420.0		39.0	n.d.	4.3				
178101	10.5	65.5	106.2	10.4	241.6	32.1	217.6	4.8	0.8	3.0	0.4	2.1	11.5	0.4	1.0		1.0	0.1	37.0	7.0		23.7	4.2	36.8	5.1	17.1	48.0	0.59	0.07
178101	8.0	56.0	88.0		208.7	28.0	210.0						13.0						15.0	6.0	n.d.	18.5	4.0	33.0	4.0	14.0	43.0		0.05
178102	6.8	24.2	40.6	4.5	288.0	17.4	169.3	3.6	1.0	3.0	0.5	2.8	15.8	0.5	1.5		1.5	0.3	84.3	27.0	n.d.	19.0	47.9	7.7	13.1	100.7	64.3	0.93	0.15
178103	22.7	106.3	183.9	18.7	238.7	61.5	438.8	9.4	1.6	5.8	0.7	3.2	176	0.6	1.3		1.3	0.2	36.2	21.8		27.2	5.9	42.5	6.7	22.3	104.4	0.62	0.12
178103	17.0	100.0	183.0		207.2	58.0	407.0	8.1					19.0						26.0	17.0	n.d.	23.2	4.0	39.0	4.0	19.0	96.0		0.08
187640	7.3	28.0	58.8	5.5	388.4	18.2	169.6	2.7	0.6	1.9	0.2	1.1	6.3	0.2	0.6		0.6	0.1				24.3		21.9	4.4				0.13
187640	5.0	22.0	36.0		314.6	15.0	140.0						8.0						7.0	2.0		20.6	9.0	17.0	5.0	20.0	52.0		0.11
187649	16.3	44.6	83.1	8.2	111.8	25.5	143.4	4.1	0.6	3.1	0.4	2.3	14.8	0.5	1.2		1.2	0.1				23.2		47.9	4.6			0.48	0.09
187649	14.0	35.0	55.0		98.4	18.0	122.0						15.0						3.0	1.0		19.8	6.0	41.0	3.0	5.0	40.0		0.09
187651	7.3	142.2	301.2	29.8	190.4	94.8	348.7	14.9	1.3	9.2	1.0	4.5	16.3	0.7	1.6		1.2	0.2				21.8		52.3	4.9			0.31	0.02
187651	4.0	160.0	273.0		156.8	86.0	282.0						19.0						2.0	4.0		18.4	8.0	44.0	4.0	13.0	48.0		0.01
187655	13.4	65.0	135.8	13.9	121.8	44.5	186.8	7.6	0.6	4.9	0.6	3.3	18.5	0.6	1.7		2.1	0.3				22.9		62.2	5.7			0.29	0.04
187655	11.0	65.0	111.0		107.1	38.0	156.0						19.0						3.0	5.0		18.4	8.0	54.0	3.0	9.0	43.0		0.04
190971	18.																												

Table A1.2. Lu–Hf analytical data for northern Murchison Domain zircon samples

Sample no-grain no. spot no	Crystallization age	$^{176}\text{Hf}/^{177}\text{Hf}$ measured	$^{176}\text{Hf}/^{177}\text{Hf}$ 1SE	$^{176}\text{Lu}/^{177}\text{Hf}$ measured	$^{176}\text{Yb}/^{177}\text{Hf}$ measured	$^{176}\text{Hf}/^{177}\text{Hf}$ initial	εHf	εHf 1 σ error	T_{DM} (crustal)	Highly metamict crystal
178102 (–26.74518 S, 118.30393 W)										
178102-03.1	2797	0.281095	0.000015	0.000635	0.019507	0.281061	2.4	0.53	3.10	
178102-07.1	2792	0.281145	0.000017	0.000851	0.027056	0.281100	3.6	0.60	3.02	
178102-11.1	2789	0.281092	0.000017	0.000821	0.023150	0.281048	1.7	0.60	3.14	
178102-13.1	2791	0.281148	0.000023	0.000942	0.030005	0.281098	3.5	0.81	3.02	
178102-17.1	2779	0.281135	0.000013	0.000921	0.028075	0.281086	2.9	0.46	3.06	
178102-18.1	2774	0.281106	0.000014	0.000885	0.025764	0.281059	1.8	0.49	3.12	
178102-19.1	2791	0.281137	0.000015	0.000898	0.029543	0.281089	3.2	0.53	3.04	
178102-26.1	2785	0.281099	0.000010	0.000763	0.022713	0.281058	2.0	0.35	3.12	
178102-30.1	2790	0.281052	0.000018	0.000946	0.030528	0.281001	0.1	0.63	3.24	
178103 (–26.734740 S, 118.264940 W)										
178103-01.1	2652	0.281122	0.000010	0.000265	0.00956	0.281109	0.71	0.35	2.91	
178103-02.1	2689	0.281059	0.000018	0.000349	0.01242	0.281041	-0.84	0.63	3.00	
178103-03.1	2785	0.281063	0.000016	0.000836	0.02778	0.281018	0.58	0.56	3.03	
178103-04.1	2659	0.281104	0.000008	0.000315	0.01115	0.281088	0.14	0.29	2.94	
178103-05.1	2642	0.281049	0.000009	0.000336	0.00957	0.281032	-2.24	0.30	3.01	
178103-06.1	2664	0.281061	0.000012	0.000268	0.01177	0.281047	-1.19	0.42	2.99	
178103-07.1	2655	0.281109	0.000010	0.000794	0.02222	0.281069	-0.64	0.35	2.97	
178103-08.1	2657	0.281084	0.000010	0.000643	0.02246	0.281051	-1.21	0.34	2.99	
178103-09.1	2655	0.281019	0.000012	0.000227	0.00928	0.281007	-2.82	0.42	3.05	
178103-10.1	2629	0.281072	0.000010	0.000323	0.01093	0.281056	-1.70	0.35	2.98	
178103-12.1	2667	0.281036	0.000017	0.000284	0.00948	0.281022	-2.04	0.60	3.03	
178103-13.1	2653	0.281073	0.000010	0.000298	0.01280	0.281058	-1.07	0.34	2.98	
178103-14.1	2647	0.281083	0.000025	0.000354	0.01290	0.281065	-0.95	0.88	2.97	
178103-15.1	2668	0.281040	0.000020	0.000206	0.00803	0.281029	-1.73	0.70	3.02	
178103-16.1	2653	0.281018	0.000016	0.000281	0.00823	0.281004	-3.00	0.56	3.05	
178103-17.1	2668	0.281055	0.000015	0.000239	0.00727	0.281043	-1.26	0.53	3.00	
178103-18.1	2649	0.281154	0.000018	0.000469	0.01593	0.281130	1.41	0.63	2.88	
178103-19.1	2654	0.281058	0.000022	0.000241	0.00707	0.281046	-1.48	0.77	2.99	
178105 (–26.88082 S, 118.48939 W)										
178105-01.1	2755	0.281067	0.000014	0.000928	0.028707	0.281018	-0.1	0.49	3.23	
178105-06.1	2753	0.281164	0.000030	0.001740	0.056004	0.281072	1.8	1.05	3.11	
178105-10.1	2775	0.281075	0.000038	0.000726	0.021802	0.281036	1.0	1.33	3.17	
178105-11.1	2752	0.281073	0.000018	0.000724	0.025650	0.281035	0.4	0.63	3.19	
178105-12.1	2755	0.281155	0.000024	0.002175	0.071147	0.281040	0.7	0.84	3.18	Yes
178105-16.1	2756	0.281148	0.000110	0.001151	0.034681	0.281087	2.4	3.85	3.07	
178141 (–27.09211 S, 118.29869 W)										
178141-04.1	2740	0.281154	0.000020	0.002514	0.078630	0.281022	-0.3	0.70	3.23	Yes
178141-08.1	2743	0.281169	0.000008	0.002447	0.086077	0.281041	0.4	0.28	3.19	Yes
178141-11.1	2742	0.281111	0.000017	0.001189	0.042832	0.281049	0.7	0.60	3.17	
178141-12.1	2755	0.281171	0.000018	0.003986	0.125045	0.280961	-2.2	0.63	3.36	Yes
178141-18.1	2756	0.281096	0.000009	0.001437	0.043941	0.281020	0.0	0.32	3.22	Yes
178141-19.1	2739	0.281119	0.000009	0.003847	0.120889	0.280917	-4.1	0.30	3.47	

Table A1.2. continued

Sample no-grain no. spot no	Crystallization age	$^{176}\text{Hf}/^{177}\text{Hf}$ measured	$^{176}\text{Hf}/^{177}\text{Hf}$ 1SE	$^{176}\text{Lu}/^{177}\text{Hf}$ measured	$^{176}\text{Yb}/^{177}\text{Hf}$ measured	$^{176}\text{Hf}/^{177}\text{Hf}$ initial	ϵHf	ϵHf 1 σ error	T_{DM} (crustal)	Highly metamict crystal
178142	(-27.03435 S, 118.38427 W)									
178142-03.1	2798	0.281086	0.000012	0.001712	0.049665	0.280994	0.0	0.42	3.25	
178142-06.1	2811	0.281045	0.000013	0.000762	0.018620	0.281004	0.7	0.46	3.22	
178142-08.1	2813	0.281077	0.000014	0.001055	0.028228	0.281020	1.3	0.49	3.18	
178142-09.1	2812	0.281072	0.000013	0.001200	0.035803	0.281007	0.8	0.46	3.21	
178142-17.1	2811	0.281051	0.000014	0.001094	0.032654	0.280992	0.3	0.49	3.25	
178142-18.1	2796	0.281021	0.000013	0.000502	0.017648	0.280994	0.0	0.46	3.26	Yes
178194	(-27.23331 S, 117.66692 W)									
178194-01.1	2737	0.281004	0.000015	0.000253	0.009238	0.280991	-1.5	0.53	3.31	Yes
178194-02.1	2751	0.280999	0.000011	0.000348	0.011015	0.280981	-1.5	0.39	3.32	Yes
178194-03.1	2744	0.281010	0.000017	0.000560	0.019905	0.280981	-1.7	0.60	3.32	Yes
178194-04.1	2742	0.280975	0.000014	0.000467	0.017793	0.280950	-2.8	0.49	3.39	Yes
178194-05.1	2749	0.280991	0.000010	0.000589	0.019336	0.280960	-2.3	0.35	3.37	Yes
178194-10.1	2747	0.280876	0.000010	0.000722	0.024458	0.280838	-6.7	0.34	3.64	
178194-11.1	2958	0.280947	0.000011	0.000591	0.017847	0.280913	0.9	0.39	3.32	Yes
178196	(-27.11973 S, 117.58999 W)									
178196-01.1	2746	0.280956	0.000015	0.000509	0.013358	0.280929	-3.5	0.53	3.44	Yes
178196-06.1	2750	0.281012	0.000014	0.000556	0.014476	0.280983	-1.5	0.49	3.31	Yes
178196-07.1	2752	0.280913	0.000025	0.000286	0.008149	0.280898	-4.5	0.88	3.50	
178196-09.1	2751	0.280950	0.000015	0.000746	0.018797	0.280911	-4.0	0.53	3.48	
178196-12.1	2747	0.280910	0.000018	0.000306	0.008391	0.280894	-4.7	0.63	3.52	Yes
178196-14.1	2752	0.280845	0.000018	0.001976	0.061986	0.280741	-10.0	0.63	3.86	
178196-17.1	2908	0.280928	0.000030	0.000506	0.015315	0.280900	-0.8	1.05	3.39	Yes
178196-18.1	2749	0.281117	0.000019	0.000442	0.013033	0.281094	2.4	0.67	3.06	Yes
178197	(-27.12437 S, 117.59108 W)									
178197-1.1	2621	0.280837	0.000015	0.000624	0.021072	0.280806	-10.8	0.53	3.80	
178197-2.1	2525	0.280885	0.000023	0.001516	0.060676	0.280812	-12.8	0.81	3.85	Yes
178197-3.1	2618	0.281012	0.000092	0.002225	0.078843	0.280901	-7.5	3.22	3.59	
178197-4.1	2633	0.280936	0.000021	0.001021	0.039851	0.280885	-7.7	0.74	3.62	
178197-5.1	2617	0.280921	0.000025	0.001169	0.045809	0.280863	-8.9	0.88	3.68	
178197-6.1	2621	0.280823	0.000017	0.000694	0.026220	0.280788	-11.4	0.60	3.84	
178197-7.1	2607	0.280871	0.000023	0.000848	0.031353	0.280829	-10.3	0.81	3.76	
178197-8.1	2623	0.280984	0.000019	0.001428	0.051611	0.280912	-6.9	0.67	3.56	
178197-10.1	2610	0.281052	0.000031	0.001853	0.070369	0.280960	-5.6	1.09	3.46	
178197-11.1	2625	0.280908	0.000019	0.001102	0.041309	0.280853	-9.0	0.67	3.69	
178197-12.1	2614	0.280824	0.000022	0.000485	0.015596	0.280800	-11.2	0.77	3.82	
178199	(-27.02381 S, 117.94078 W)									
178199-01.1	2665	0.281128	0.000014	0.000660	0.023123	0.281094	0.5	0.49	3.12	
178199-07.1	2679	0.281086	0.000014	0.000678	0.021296	0.281051	-0.7	0.49	3.21	
178199-08.1	2690	0.281072	0.000015	0.000777	0.023213	0.281032	-1.1	0.53	3.24	
178199-09.1	2671	0.281077	0.000011	0.000153	0.003309	0.281069	-0.3	0.39	3.17	

Table A1.2. continued

Sample no-grain no. spot no	Crystallization age	$^{176}\text{Hf}/^{177}\text{Hf}$ measured	$^{176}\text{Hf}/^{177}\text{Hf}$ 1SE	$^{176}\text{Lu}/^{177}\text{Hf}$ measured	$^{176}\text{Yb}/^{177}\text{Hf}$ measured	$^{176}\text{Hf}/^{177}\text{Hf}$ initial	ϵHf	ϵHf 1 σ error	T_{DM} (crustal)	Highly metamict crystal
178199-10.1	2678	0.281114	0.000011	0.000294	0.008044	0.281099	1.0	0.39	3.10	
178199-12.1	2684	0.281089	0.000009	0.000502	0.014248	0.281063	-0.2	0.33	3.18	
178199-15.1	2670	0.281119	0.000015	0.000640	0.018552	0.281086	0.3	0.53	3.14	
178199-16.1	2674	0.281071	0.000019	0.000492	0.013671	0.281046	-1.0	0.67	3.22	
178199-17.1	2668	0.281058	0.000014	0.001511	0.045177	0.280981	-3.5	0.49	3.38	
185922 (-27.35250 S, 117.82600 W)										
185922-01.1	2717	0.281119	0.000036	0.003383	0.101422	0.280943	-3.7	1.26	3.43	
185922-03.1	2734	0.281134	0.000025	0.001623	0.040383	0.281049	0.5	0.88	3.17	
185922-05.2	2739	0.281253	0.000040	0.005920	0.217817	0.280943	-3.2	1.40	3.41	
185922-06.1	2731	0.281264	0.000021	0.004808	0.175360	0.281013	-0.9	0.74	3.26	
185922-09.1	2728	0.281144	0.000033	0.002944	0.082342	0.280990	-1.7	1.16	3.31	
185922-10.1	2735	0.281164	0.000030	0.007022	0.193914	0.280797	-8.5	1.05	3.75	
185922-11.1	2723	0.281190	0.000018	0.004336	0.119432	0.280964	-2.8	0.63	3.38	Yes
185922-13.1	2732	0.281188	0.000044	0.004133	0.118231	0.280972	-2.3	1.54	3.35	
185923 (-27.41191 S, 117.69617 W)										
185923-01.1	2726	0.281108	0.000013	0.001737	0.052859	0.281017	-0.8	0.46	3.25	Yes
185923-04.1	2725	0.281114	0.000012	0.001698	0.052862	0.281025	-0.6	0.42	3.23	Yes
185923-07.1	2729	0.281125	0.000012	0.000920	0.027837	0.281077	1.4	0.42	3.11	Yes
185923-11.1	2718	0.281153	0.000014	0.001100	0.034175	0.281096	1.8	0.49	3.08	Yes
185923-12.1	2726	0.281089	0.000009	0.001182	0.037782	0.281027	-0.5	0.33	3.23	
185923-15.1	2720	0.281121	0.000015	0.001856	0.060994	0.281024	-0.7	0.53	3.24	Yes
185927 (-26.79899 S, 117.99168 W)										
185927-01.1	2715	0.281147	0.000013	0.001037	0.035035	0.281093	1.6	0.46	3.09	
185927-03.1	2708	0.281163	0.000012	0.001673	0.059623	0.281076	0.9	0.42	3.13	
185927-06.1	2712	0.281152	0.000011	0.001576	0.059487	0.281070	0.7	0.39	3.14	Yes
185927-09.1	2717	0.281162	0.000011	0.002245	0.081699	0.281045	0.0	0.39	3.20	Yes
185927-12.1	2707	0.281165	0.000010	0.001843	0.066305	0.281070	0.6	0.34	3.15	Yes
185927-16.1	2709	0.281200	0.000010	0.002275	0.082258	0.281082	1.1	0.35	3.12	Yes
185927-21.1	2712	0.281149	0.000009	0.001763	0.061510	0.281058	0.3	0.32	3.17	Yes
185927-26.1	2708	0.281131	0.000011	0.001502	0.051537	0.281053	0.0	0.39	3.18	Yes
185927-29.1	2710	0.281133	0.000012	0.002174	0.078998	0.281020	-1.1	0.42	3.26	Yes
S185929 (-26.69758 S, 117.97422 W)										
185929-1.1	2603	0.281030	0.000010	0.001570	0.064806	0.280952	-6.0	0.35	3.49	
185929-4.1	2611	0.280868	0.000014	0.000848	0.038536	0.280826	-10.3	0.49	3.77	
185929-5.1	2600	0.281017	0.000009	0.000620	0.025504	0.280986	-4.8	0.33	3.41	
185929-6.1	2605	0.281017	0.000014	0.000726	0.022961	0.280981	-4.9	0.49	3.42	
185929-7.1	2605	0.281032	0.000011	0.002417	0.096243	0.280912	-7.4	0.39	3.58	
185929-8.1	2608	0.281003	0.000009	0.000936	0.040060	0.280956	-5.7	0.30	3.47	
185929-10.1	2603	0.280994	0.000014	0.000534	0.020575	0.280967	-5.5	0.49	3.45	
185929-11.1	2599	0.281022	0.000011	0.002059	0.084278	0.280920	-7.2	0.39	3.56	
185929-12.1	2634	0.281005	0.000023	0.000642	0.029536	0.280973	-4.6	0.81	3.42	
185929-14.1	2614	0.280982	0.000012	0.001102	0.044156	0.280927	-6.6	0.42	3.54	

Table A1.2. continued

Sample no-grain no. spot no	Crystallization age	$^{176}\text{Hf}/^{177}\text{Hf}$ measured	$^{176}\text{Hf}/^{177}\text{Hf}$ 1SE	$^{176}\text{Lu}/^{177}\text{Hf}$ measured	$^{176}\text{Yb}/^{177}\text{Hf}$ measured	$^{176}\text{Hf}/^{177}\text{Hf}$ initial	εHf	εHf 1 σ error	T_{DM} (crustal)	Highly metamict crystal
185932 (-27.34057 S, 118.17560 W)										
185932-02.1	2739	0.281089	0.000014	0.003070	0.104941	0.280928	-3.7	0.49	3.45	
185932-03.1	2747	0.281126	0.000013	0.001171	0.029908	0.281064	1.3	0.46	3.13	
185932-05.1	2746	0.281107	0.000015	0.001662	0.044837	0.281020	-0.3	0.53	3.23	
185932-08.1	2737	0.281066	0.000014	0.001811	0.047625	0.280971	-2.2	0.49	3.35	
185932-09.1	2751	0.281138	0.000010	0.001589	0.041040	0.281054	1.1	0.35	3.15	
185932-11.1	2749	0.281127	0.000015	0.002076	0.054872	0.281018	-0.3	0.53	3.24	
185933 (-27.34887 S, 118.16280 W)										
185933-05.1	2755	0.281119	0.000016	0.001590	0.042401	0.281035	0.5	0.56	3.19	Yes
185933-06.1	2768	0.281116	0.000014	0.001581	0.046650	0.281032	0.7	0.49	3.19	Yes
185933-07.1	2758	0.281129	0.000011	0.001749	0.052700	0.281037	0.6	0.39	3.19	Yes
185933-17.1	2751	0.281153	0.000012	0.001927	0.061715	0.281052	1.0	0.42	3.16	Yes
185933-24.1	2768	0.281106	0.000012	0.001750	0.055109	0.281013	0.0	0.42	3.23	Yes
185933-25.1	2767	0.281128	0.000016	0.002421	0.069979	0.281000	-0.5	0.56	3.26	Yes
185933-27.1	2749	0.281081	0.000010	0.001744	0.055680	0.280989	-1.3	0.35	3.30	Yes
185933-31.1	2768	0.281147	0.000010	0.002545	0.083464	0.281012	0.0	0.35	3.23	Yes
193972 (-26.971510 S, 117.526370 W)										
193972-01.1	2975	0.280997	0.000015	0.002657	0.11101	0.280845	-1.16	0.53	3.28	
193972-03.1	2980	0.281024	0.000024	0.001645	0.07206	0.280930	1.97	0.84	3.15	
193972-06.1	2979	0.280963	0.000020	0.001676	0.06427	0.280867	-0.28	0.70	3.24	
193972-07.1	2982	0.281009	0.000023	0.001986	0.07182	0.280895	0.78	0.81	3.20	
193972-09.1	2978	0.280979	0.000013	0.001753	0.06232	0.280879	0.10	0.46	3.22	
193972-10.1	2984	0.281022	0.000021	0.002587	0.09862	0.280874	0.08	0.74	3.24	
193972-11.1	2977	0.281006	0.000023	0.002608	0.11279	0.280857	-0.70	0.81	3.26	
193972-12.1	2978	0.280990	0.000016	0.003744	0.18913	0.280776	-3.55	0.56	3.39	
193972-13.1	2978	0.281044	0.000024	0.002789	0.12232	0.280885	0.30	0.84	3.22	
193972-14.1	2971	0.280968	0.000017	0.001256	0.04294	0.280896	0.58	0.60	3.20	
193972-15.1	2978	0.281000	0.000018	0.001316	0.05601	0.280925	1.75	0.63	3.16	
193972-16.1	2980	0.280908	0.000017	0.001621	0.07676	0.280815	-2.11	0.60	3.31	
193972-17.1	2975	0.280985	0.000020	0.002654	0.09157	0.280834	-1.58	0.70	3.29	
193972-18.1	2986	0.280941	0.000010	0.000667	0.02094	0.280903	1.15	0.35	3.18	

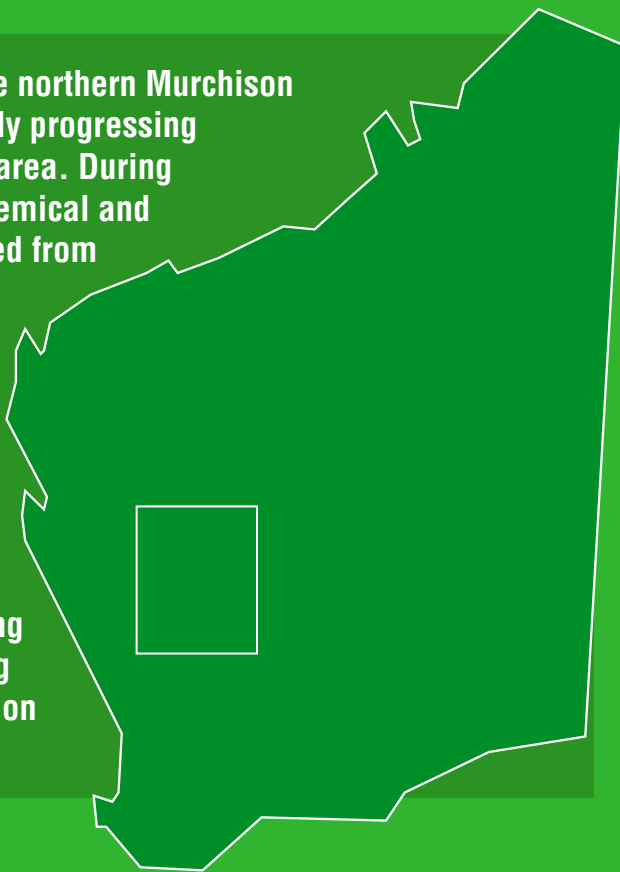
Table A1.3. Major and trace element modelling for generation of the Cullculi Suite. Results shown in Figure 8

		Cs	Rb	Ba	Th	Nb	La	Ce	Pr	Sr	Nd	Zr	Sm	Eu	Gd	Tb
	Primitive mantle normalised composition															
Cullculi Suite mafic clotty tonalite (178141)	1	229.114	59.843	80.584	93.294	8.135	36.870	25.623	18.297	14.005	13.951	12.232	8.198	6.387	5.889	5.926
Annean Supersuite granitic (178194)	2	493.671	409.449	351.982	260.000	7.714	53.712	42.197	31.014	30.664	22.674		11.599	7.440	6.040	3.704
Average Meekatharra Formation basaltic (Van Kranendonk et al., in press)	3		4.567	10.976	14.216	4.463	6.935	6.957	5.475	4.485	6.179	4.998	4.845	4.820	4.676	5.000
50:50 binary mixing of Composition 2 & Composition 3	4	493.671	207.008	181.479	137.108	6.088	30.323	24.577	18.245	17.574	14.426	4.998	8.222	6.130	5.358	4.352
75:25 binary mixing of Composition 2 & Composition 3	5	370.253	308.228	266.730	198.554	6.901	42.018	33.387	24.630	24.119	18.550	1.249	9.911	6.785	5.699	4.028

Table A1.2. continued

		<i>Primitive mantle normalised composition</i>	<i>Dy</i>	<i>Y</i>	<i>Ho</i>	<i>Er</i>	<i>Yb</i>	<i>Lu</i>	<i>TiO₂</i>	<i>Al₂O₃</i>	<i>CaO</i>	<i>Fe₂O₃T</i>	<i>SiO₂</i>	<i>MgO</i>
	1		4.098	3.956	4.207	3.500	3.611	3.514	6.434	3.204	1.062	0.686	1.366	0.136
Cullulli Suite mafic clotty tonalite (178141)														
	2		2.374	2.088	1.951	1.563	1.521	1.351	1.641	3.332	0.238	0.148	1.584	0.005
Annean Supersuite granitic (178194)														
	3		4.375	4.672	4.499	4.505	4.710	4.958	9.395	3.034	3.066	1.326	1.136	0.178
Average Meekatharra Formation basaltic (Van Kranendonk et al., in press)														
	4		3.375	3.380	3.225	3.034	3.115	3.155	5.518	3.183	1.652	0.737	1.360	0.092
50:50 binary mixing of Composition 2 & Composition 3														
	5		2.875	2.734	2.588	2.298	2.318	2.253	3.579	3.257	0.945	0.443	1.472	0.049
75:25 binary mixing of Composition 2 & Composition 3														

Regional mapping at 1:100 000 scale of the northern Murchison domain commenced in 2006 and is currently progressing southwards towards the Yalgoo–Singleton area. During the mapping program, a substantial geochemical and geochronological dataset has been analysed from hundreds of rock samples. These new data have allowed progress to be made in the understanding of the geological evolution of the domain. This has included a new stratigraphic and structural framework. This Report indicates new evidence for crustal evolution for the domain and its relation to older basement rocks. A major outcome is that a progressively fractionating sequence of granitic rocks shows reworking of older crust culminating in the cratonization of the domain.



Further details of geological products and maps produced by the Geological Survey of Western Australia are available from:

Information Centre
Department of Mines and Petroleum
100 Plain Street
EAST PERTH WA 6004
Phone: (08) 9222 3459 Fax: (08) 9222 3444
<http://www.dmp.wa.gov.au/GSWApublications>